Author/s:
Brydon, SC;da Silva, G;White, JM

Title:
Evidence that pi-ligand exchange reactions of chalcogen iranium ions proceed via Huckel pseudocoarctate transition states

Date:
2020-12

Citation:
Brydon, S. C., da Silva, G. & White, J. M. (2020). Evidence that pi-ligand exchange reactions of chalcogen iranium ions proceed via Huckel pseudocoarctate transition states. Journal of Physical Organic Chemistry, 33 (12), https://doi.org/10.1002/poc.4111.

Evidence that π-Ligand Exchange Reactions of Chalcogen Iranium Ions Proceed *via* Hückel Pseudocoarctate Transition States

Samuel C. Brydon[a*], Gabriel da Silva[b], Jonathan M. White[a*]

[a] *School of Chemistry and Bio21 Institute, The University of Melbourne, Parkville, Victoria 3010, Australia.*

[b] *Chemical Engineering, The University of Melbourne, Parkville, Victoria 3010, Australia.*

Email:

brydons@student.unimelb.edu.au

whitejm@unimelb.edu.au

Abstract

Despite numerous computational and experimental studies on the π-ligand exchange reactions of chalcogen iranium ions, a classification of the reaction class has yet to be made. The characteristics of the transition states presented thus far suggested a coarctate nature with two bonds breaking and forming simultaneously at the chalcogen centre. The change in barrier height, depending on the nature of the chalcogen and the alkene, was initially attributed as a shift in the degree of aromaticity moving from pseudocoarctate to coarctate reactions. However, this paper suggests that all twelve reactions under consideration are pseudocoarctate with a Hückel number of delocalised π electrons based on comprehensive studies of the orbital interactions and magnetic properties both at the transition state and along the reaction path. The change in barrier height was largely driven by the electrophilicity of the chalcogen and the strain present in the three-membered ring, rather than a shift in the degree of aromaticity.

Introduction

Chalcogen (Ch) iranium ions of general structure **1** have been shown to be important reactive intermediates in a variety of transformations, particularly in the functionalisation of alkenes,[1-9] and have been structurally characterised by both NMR and crystallographic techniques.[10-12] In stereoselective syntheses, neighbouring group participation by the chalcogen ensures stereochemical integrity is maintained in products **2** or **2'** following ring opening by either an inter- or intramolecular nucleophile (**Path A**, **Scheme 1**).[2,13-15] Racemisation may occur by several pathways including ring opening of the intermediate followed by bond rotation (**Path B**, **Scheme 1**), or π-ligand exchange reactions involving two distinct mechanisms.[8,12,16-18] The dissociative pathway has been controlled by utilising dry, non-coordinating solvents and non-nucleophilic counterions to avoid production of an electrophilic transfer reagent **3** between alkenes (**Path C** and **Path D**, **Scheme 1**).[11,12] The associative pathway, involving attack at the electrophilic chalcogen by another alkene equivalent, has been studied by Denmark *et al.* in solution by generating both thiiranium and seleniranium ions *in situ* and shown to be feasible for all reactions studied where there was a thermodynamic driving force (**Path E**, **Scheme 1**).[12] Studies on the stereoselective outcomes of reactions that proceed *via* these intermediates have shown this latter pathway may also be suppressed by suitably sterically bulky (e.g. 2,4,6-tri-*tert*-butylphenyl) or electron withdrawing groups (e.g. *o*-nitrophenyl) on the chalcogen (**Path E**, **Scheme 1**).[7,19-21] Though these racemisation pathways are less important for thiiranium ions, they are significant in the more electrophilic seleniranium ions and telluriranium ions and the nature of their mechanism warrants further investigation.

Recent experimental studies into cyclisations have highlighted the fact that the associative mechanism of π-ligand exchange may be exploited in synthesis rather than merely being an undesirable side reaction.[22] Continuing from similar utilisation of bromiranium salts,[23] Bock *et al*. have used both adamantyl (Ad) derived thiiranium and seleniranium ion salts to induce polyene type cyclisations *via* associative transfer of the chalcogen moiety with the diastereoselectivity in the product **6** dictated by the Eschenmoser-Stork postulate (**Scheme 2**).[11] The yields increased in the order *n*-$BuSe^+$ < PhS^+ < PhSe reflecting the influence of both the R group and the nature of the chalcogen on the extent of the transfer. These studies have prompted further investigation into the stereoelectronic factors governing the mechanism of this associative transfer.

To avoid potential dissociative transfer facilitated by solvents, counter ions and impurities, studies in the gas phase have investigated both the thermodynamic and kinetic factors controlling associative transfer (or lack thereof) of PhS^+, $PhSe^+$ and $PhTe^+$ moieties between alkenes (**Scheme 3**).[24-26] Structures of the iranium ions **27-28** in particular, produced by electrospray ionisation (ESI) of appropriate precursors **25-26**, were supported by high-resolution mass spectrometry (HRMS), infrared multiple photon dissociation (IRMPD) and density functional theory (DFT) calculations with little if any isomerisation to the related onium ions occurring.[24,25] Thiiranium ions **10**, **19**, and **27** were not observed to undergo transfer in the gas phase and instead produced an electrophilic addition product, contrasting with experiments by Denmark *et al*. which suggest this transfer is feasible in the solution phase.[12] Where there was a thermodynamic driving force, the $PhSe^+$ moiety was transferred between alkenes in ion-molecule reactions (IMR) (**28** to **30**), but identity exchange reactions suggested that the intrinsic kinetic barrier could also dominate reaction outcomes (**11** to **14** compared to **20** to **23**). Both telluriranium ions **12** and **21** readily underwent associative π-ligand exchange reflecting the greater electrophilicity of this chalcogen atom. DFT calculations suggested that the identity exchange of **21** to **24** is effectively barrierless in the gas phase as, though a transition state was identified for this reaction, its energy was so low compared to the ion-neutral complex that the barrier vanished once zero point vibrational energy corrections were applied.[26]

Despite these insights, no studies have determined the nature of the transition states of associative π-ligand exchange of chalcogen iranium ions. Previous computational work has shown that there are two significant orbital interactions,[18] with donation of the π orbitals of the alkenes into a vacant p^+ orbital on the chalcogen and a weaker back-bonding of the chalcogen p-type lone pair into the π* orbitals of the alkenes, analogous to π back-bonding in metal complexes with alkene ligands (**Figure 1**).[27] These interactions dictate the coplanar orientation of the π orbitals of the alkenes at the transition state to ensure optimal orbital overlap, leading to comparisons in the topology to the triple ion configuration in S_N2 reactions ($X^- \cdots CH_3^+ \cdots X^-$). At first, the concomitant bond breaking and forming may suggest a transition state of pericyclic nature. However, pericyclic reactions involve one bond breaking and forming per atom, whilst in this case there are each two bonds breaking and forming at the central chalcogen suggesting these transition states may instead be coarctate in nature.

Coarctate transition states have been determined as topologically equivalent to pericyclic transition states (homeomorphous), thus the same Hückel and Möbius rules may be applied to determine aromaticity or antiaromaticity (or lack thereof in pseudopericyclic transition states) may be applied to coarctate transition states as well.[28,29] Herges has shown that coarctate reactions with $4n + 2$ π electrons (Hückel) exhibit coplanar loops, whilst reactions with $4n$ π electrons (Möbius) exhibit orthogonal loops.[29,30] An electron count of the π-ligand exchange transition states reveals a total of 6 π electrons involved ($2 \times \pi_{C=C}$ and $1 \times n_{Ch}$, i.e. $4n + 2$), suggesting potential Hückel aromaticity. Application of group theory has been used to discriminate between pseudo and true pericyclic and coarctate transition states, as there must be distortion in the orbital arrangement (e.g. C_2 symmetry) to ensure there are no disconnections in the latter. However, a high symmetry point group in the molecule (e.g. D_{2h}), particularly in the plane where the bond breaking and forming is occurring, suggests some level of disconnection in the orbital loop and hence these transition states are more likely pseudopericyclic or pseudocoarctate in nature.[30]

Computational Methods

Density functional theory (DFT) calculations were carried out with the Gaussian 16 revision *B.01* software package.[31] Geometries were optimised using the hybrid meta-GGA functional M06-2X and the def2-TZVP basis set,[32,33] which has been used previously for the study of chalcogen iranium ions and provided theoretical rates in excellent agreement with gas phase experiments.[25,26] The M06-2X functional is suitable for main group thermochemistry with reliability across a range of data sets compared to other DFT methods,[34] and similar functionals (M05-2X) have accurately predicted the structure of asymmetric oxiranium ions compared to the high-level coupled-cluster CCSD method.[35] Zero-point vibrational energy (ZPVE) corrections for electronic energies were obtained using unscaled harmonic vibrational frequencies. Transition states were confirmed by frequency analysis (one imaginary frequency) and connected to the intermediates by intrinsic reaction coordinate (IRC) calculations. Unless otherwise noted, energies in the text include ZPVE corrections and are at 0 K. The reaction energy (ΔE) has been noted by Dau *et al* as the pertinent thermodynamic parameter to describe low pressure bimolecular reactions and as such has been used in this study.[36] Cartesian coordinates for all calculated structures as well as enthalpies and Gibbs energies (298 K) are available in the Supporting Information. Natural bond orbital (NBO) analysis of transition states and selected reaction coordinates was conducted with NBO 7.0 developed by Glendening and co-workers,[37] and orbitals visualised with Avogadro version 1.2.0.[38] Stabilisation energies were obtained by deletions analysis through removal of individual significant orbital interactions in the NBO program interfaced with Gaussian 16 (see text for further information).[39] Points along the reaction coordinate (obtained from IRC calculations) were examined by NBO, whilst the magnetic properties were monitored by changes in the anisotropy of the magnetic susceptibility (χ_{anis}) calculated using the individual gauges for atoms in molecules (IGAIM)

method.[40] Further information about the electron delocalisation at the transition state was obtained by analysing the anisotropy of the induced current density (ACID) calculated using the ACID program provided by the Herges research group.[41] The current densities were calculated using the continuous set of gauge transformation (CSGT) method.[42] All NBO, IGAIM and ACID calculations were performed with the M06-2X/def2-TZVP method.

Results and Discussion

Reaction Pathways

The choice of systems to investigate associative π-ligand exchange transition states with the above tools includes those studied both theoretically and experimentally in the gas phase previously.[18,24-26] These are outlined in **Scheme 4** with an array of both identity and non-identity exchange reactions bringing the total to twelve systems.

Variation in the R group on the chalcogen from H to Ph and its impact on the transfer between ethene molecules was first studied, reflecting both Solling *et al.* earlier theoretical study and those later studied in the gas phase (**A** and **B**, **Scheme 4**).[18,26] This has been continued by varying the alkenes to cyclohexene molecules as previously explored with a phenyl group on the chalcogen (**C**, **Scheme 4**).[26] For reactions **B** and **C**, no level of deuteration has been included as was required to be monitored in the gas phase, removing potential deuterium isotope effects and making the systems identity reactions according to IUPAC.[43] Of the final three non-identity reactions involving transfer of $PhCh^+$ from styrene to cyclohexene, the sulphur and selenium systems have been studied previously (**D**, **Scheme 4**).[24,25] Though the telluriranium reaction **D3** has not been studied experimentally, it is included here for completeness.

The simplest system was that first studied by Solling, Wild and Radom in which the HS^+ moiety was transferred between two ethenes in an identity exchange reaction (**A1**, **Scheme 4**). This has been extended in the present study to include the transfer of HSe^+ and HTe^+ between two ethene molecules (**A2** and **A3** respectively, **Scheme 4**). The first step in the reaction involves the barrierless formation of the ion-neutral association complex, making the subsequent transfer of the chalcogen moiety the rate determining step. The following ion-neutral dissociation complex for the identity reactions are the same due to symmetry (and were not calculated separately) making these reactions an example of the Brauman double energy well.[26,44] As a comparison to Radom's calculations, the electronic energy of the association complex and transition state for HS^+ exchange relative to the reactants was found to be within 2 kJ mol^{-1} of the previous study, reinforcing the accuracy of the M06-2X/def2-TZVP level of theory compared to the high level G2 (ZPE = MP2) theory (**A1**, **Table 1**). Of the three systems, the sulphur moiety transfer is predicted not to occur in the gas phase ($\Delta E^{\ddagger}$ = +48.2 kJ mol^{-1}) under standard linear ion-trap mass spectrometry conditions described previously,[26] whilst the tellurium reaction would readily proceed ($\Delta E^{\ddagger}$ = -32.7 kJ mol^{-1}). The selenium reaction is more difficult to predict, as although the energy of the transition state is slightly above the energy of the system as defined by the energy of the reactants ($\Delta E^{\ddagger}$ = +6.8 kJ mol^{-1}), ion-molecule reactions with calculated barriers up to approximately 9-10 kJ mol^{-1} relative to the reactants may still be observed in the gas phase at room temperature,[45] likely due to a Boltzmann distribution of reactant ion energies and collisions with the helium bath gas. Indeed, the barrier to electrophilic addition of cyclohexene to thiiranium ion **27** has previously been calculated at +5 kJ mol^{-1} at the M06-2X/def2-TZVP level of theory, but was observed to proceed with a relatively slow rate coefficient of 3.7×10^{-14} cm^3 $molecule^{-1}$ s^{-1} in a linear ion trap quadrupole (LTQ) mass spectrometer.[25] The S_N2 reaction of $^{37}Cl^-$ with $CH_3{}^{35}Cl$ has also been shown to proceed with a rate coefficient of 3.5×10^{-14} cm^3 $molecule^{-1}$ s^{-1} in an ion cyclotron resonance (ICR) spectrometer,[46] despite a calculated barrier of +9.8 kJ mol^{-1} relative to the free reactant energies at the G2 level of theory.[45]

The trend of decreasing barriers to π-ligand exchange moving down the chalcogens has mostly been attributed to the increasing electrophilicity of the chalcogen from sulphur to tellurium. However, the topology of the association complex between the incoming alkene and the iranium ion was also identified as another indicator for whether the reaction would proceed or not.[26] In the previous study on chalcogen iranium ion identity reactions (see **Scheme 3**), if the orientation of the π orbitals of the alkenes were close to being coplanar in the complex, mirroring the orbital topology in the transition state, then the reaction was predicted to proceed, with both DFT calculations and experimental observations in agreement. However, if the π orbital of the incoming alkene donated into a $\sigma^*_{Ch\text{-}C}$ orbital to form chalcogen bond-like interaction, then the reaction was predicted not to occur and indeed no product formation was observed. Despite the high barrier of + 48.2 kJ mol^{-1} for reaction **A1**, the calculated orientation of the π orbital of ethene relative to the thiiranium ion in complex **31a** is not towards a $\sigma^*_{S\text{-}C}$ orbital. Nevertheless, there is significant deviation from the orientation of the alkene π orbitals observed in the transition state **31b** (**Figure 2**). Indeed, looking at the side-on view, the difference in the $C{=}C_{mid}$ – Ch – $C{=}C_{mid}$ angle between the complexes **31a**-**33a** and the transition states **31b**-**33b** reduces going down the group ($\Delta\theta_S = 7.8° > \Delta\theta_{Se} = 2.6° > \Delta\theta_{Te} = 0.3°$). As shown previously with NBO calculations, this similar topology in the complex reflects the orbitals involved being in an orientation closer to that of the transition state and thus less energy is required for the reaction to proceed.[26] This trend is also observable in the difference between the Ch-C bond lengths (amongst other structural parameters) in the complex and those in the transition state with the telluriranium ion complex **33a** being most like its corresponding transition state **33b** (**Figure 2**).

Comparing to previous calculations by Solling *et al.* on the topology of the complex relative to that of the transition state, however, reveals that their calculated complex placed the π orbitals of the alkenes orthogonal to one another, whilst they were coplanar in the transition state.[18] Despite the similarity in the calculated energies as mentioned, MP2 has been shown to occasionally incorrectly optimise geometries or miss some minima, such as the benzenium-ethene complex, due to overestimation of electron correlation of double excitations in delocalised systems.[47] Alternatively, the potential energy surface of complex formation may be rather shallow with several possible minima available, and we have previously suggested that there would be rapid interconversion between the two potential chalcogen bond-like interactions in some of these complexes.[26] Nevertheless, for π-ligand exchange of chalcogen iranium ions to occur the π orbitals of the alkenes must become coplanar, hence the complexes calculated in this study appear to be the more likely ones for the reactions to proceed through.

The energy surfaces of the identity reactions shown in reactions **B** and **C** have been analysed in detail previously for the corresponding deuterated system, and there is excellent agreement between the two (**Table 1**). The overall trend of the barrier heights decreasing down the group is observed within each reaction, noting the barrier to $PhSe^+$ exchange between cyclohexenes in **C2** is lower than the combined reactant energies ($\Delta E^{\ddagger}$ = -8.7 kJ mol^{-1}) compared to exchange between ethenes in **B2** as discussed in the previous study.[26] Comparing the effects of changing the R substituent from a hydrogen (**A**) to a phenyl group (**B**) shows an increase in barrier heights for the latter most likely due to an increase in the steric hindrance to the incoming alkene (**Table 1**). Further studies are necessary to investigate the effects of the R group substituent on π-ligand exchange in the gas phase, and if they correlate with studies mentioned earlier in the condensed phase,[7,19] but this is beyond the scope of this work.

Figure 3 shows the set of non-identity reactions **D1**-**3** under consideration with the exchange of the chalcogen moiety from styrene to cyclohexene overall exoergic. The reaction of thiiranium ion **27** with cyclohexene has been shown not to occur in the gas phase as expected based on the modest barrier of +28.2 kJ mol^{-1} (Black, **Figure 3**).[25] The selenium pathway has been shown experimentally to occur with a rate of 6.6×10^{-13} cm^3 molecule^{-1} s^{-1},[24] though the relative energy surface mapped out in this study does not agree well with the same one calculated previously at the M06/6-31+G(d) level of theory with

discrepancies of up to 35 kJ mol^{-1} (Red, **Figure 3**), noting the latter were reported at 298 K. The surface determined in this study is likely more reliable as we have shown in **Table 1** that the M06-2X/def2-TZVP level of theory produced results in excellent agreement with the high level G2 (ZPE = MP2) theory, and from previous work RRKM theoretical rates based upon energy surfaces calculated at M06-2X/def2-TZVP were in good agreement with experimental rates of π-ligand exchange in the gas phase.[26]

The association complex **28a** differs to the one previously calculated in reference 24 as the π orbitals of the alkenes are slightly twisted relative to one another rather than adopting the $\pi_{C=C}$ - σ^*_{Se-C} chalcogen bond-like interaction such as in the thiiranium ion complex **27a**. This previous complex has been recalculated at the current level of theory and the energetic difference between complex **28a** and **28a'** is only 1.1 kJ mol^{-1} with a transition state **28a''** connecting the two isomers with a barrier of 1.8 kJ mol^{-1} (**Scheme 5**). With a margin of error of ± 5 kJ mol^{-1} for similar theoretical methods,[48] the conversion between the two may be considered barrierless and not the rate determining step. Despite the potential for both association complexes **28a** and **28a'** to form, the rate determining exchange reaction must proceed *via* **28a** from the IRC calculations, making this complex the only one considered in further analysis.

There are some shifts in the non-identity reaction trends compared to the previous identity reactions detailed above in **Figure 3**. The change in orientation of the π orbitals in the association complex is as expected based on the relative heights of the transition states with **28a** and **34a** closer to the topology of **28b** and **34b**, i.e. more coplanar, than in the case of the sulphur association complex **27a** and transition state **27b**. However, the dissociation complexes are less like the transition states as predicted by the Hammond postulate for exoergic reactions (if the complexes are viewed as reactant and product for the rate determining step). In addition, the trend in energies of the products is reversed compared to the association complexes and transition states with the telluriranium ion **34** reaction with cyclohexene nearing thermoneutrality. The rates of reactions of seleniranium ions with cycloalkenes of differing ring size have been shown previously to increase with the release of ring strain.[24] In this reaction, though there is likely some enthalpic force driving formation of the conjugated π system in styrene, the ring strain release between styryl derived telluriranium ion **34** and cyclohexyl derived telluriranium ion **21'** is likely smaller than that between the corresponding thiiranium ions **27** and **19'** and seleniranium ions **28** and **20'**. The C-Ch-C angle of the iranium ion core may be taken as a marker of ring strain, and indeed the difference between the C-Te-C angles for **34** and **21'** is only 0.1° compared to 0.8° and 0.7° for the corresponding selenium and sulphur systems. This is partially due to the increased donation of the styryl π-system into the neighbouring σ^*_{C-Te} orbital ($E(2)$ = 37 kcal mol^{-1} from NBO analysis), leading to an increase in the benzylic carbon – tellurium bond length and hence less ring strain in the reactant ion **34** compared to the others.

Birney *et al.* have shown that pseudopericyclic transition states of a range of reactions (particularly electrocyclic ring openings and cycloadditions) would have symmetry allowed, near-planar transition states with very low energetic barriers.[49-51] These characteristics may be investigated in this study for potential pseudocoarctate transition states with the activation energy the difference between the association complex and transition states energies, whilst the planarity may be assessed by the $C{=}C_{mid}$ – Ch – $C{=}C_{mid}$ angle across the dual three-membered ring system. Upon examination, however, there was no clear trend between these two variables (R^2=0.008) with the selenium systems being the most planar in reactions **B2**, **C2** and **D2** (**Table 2**). Based upon the structure reactivity relationship of the electrocyclic ring openings and cycloaddition reactions, the highest barrier reactions involving the smaller thiiranium systems would be expected to be the least planar and most aromatic with the large telluriranium ion systems exhibiting the opposite features. However, this is not the case and hence this structure reactivity correlation is not an adequate explanation for these systems, perhaps suggesting that

a shift in the degree of aromaticity may not be a driving force behind the change in reaction barrier height.

Nevertheless, there are some trends between the barrier heights and some other geometric properties of the transition states, namely the related C-Ch bond length and the C-Ch-C angle within each three-membered ring. Indeed, each of these parameters against the barrier heights yield R^2 values of 0.825 and 0.808 respectively and removing the outlier of reaction **B1** (points on the far right hand side in **Figure 4**) increases the R^2 to 0.900 (bond length) and 0.893 (angle). The two parameters are not quite interdependent as the discrepancies in the R^2 values may be attributed to the slight change in the iranium C-C bond length affecting the C-Ch-C angle (see, for example, **Figure 2**). The trend in ring strain suggests that the small thiiranium ions are less reactive as they are less strained, compared to the larger telluriranium ions, and thus require more energy to transfer the chalcogen moiety to another alkene. The change in bond lengths also implies that less energy is needed to break the longer (weaker) bonds in the larger telluriranium ions leading to lower barriers for π-ligand exchange. Further examination of the orbital interactions by NBO analysis corroborate these initial findings (*vide infra*) and provides further insight into whether or not these changes are due to shifts in the degree of aromaticity.

Transition states have a high extent of electron delocalisation, particularly in these types of concerted reactions, meaning one Lewis structure is not an appropriate descriptor. Instead, natural resonance theory (NRT) may be used to examine the different types of Lewis structures that contribute to the overall delocalised structure. For example, analysis of the simplest transition states **31b-33b** in reactions **A1-3** highlights the increase in positive charge placed on the chalcogen going down the group from sulphur (4.78%) to selenium (4.87%) to tellurium (12.34%) reflecting polarizability trends down the group (**Figure 5**). The most significant structures place the positive charge on the carbons rather than the chalcogen as shown in **Figure 5**, but there are minor (about 20-30%) contributors that assist in distributing the charge further onto the hydrogens of the ethyl moieties (see **Tables S1-3** in the Supporting Information for the NRT output).

The introduction of the phenyl group on the chalcogen and cyclohexyl/styryl moieties further distributes the charge leading to even greater delocalisation. However, analysis of all the potential resonance structures is unnecessary as natural charge analysis offers a more efficient and quantitative method to evaluate the degree of positive charge on the chalcogen. As mentioned earlier, the electrophilicity of the chalcogen has been suggested as one of the major drivers in these exchange reactions and this would be expected to reflect the barrier height of the reactions under study. A comparison of these variables produces a correlation with $R^2 = 0.6318$ (**Figure 6**), supporting electrophilicity as a significant driver, but not the sole predictive indicator.

The strength of orbital interactions are usually evaluated by the second order perturbation energy, however, initial calculations produced values beyond the second order perturbation limit (>100 kcal mol^{-1}),[39] in particular for the primary $\pi_{C=C} - p^{+}_{Ch}$ interactions. As mentioned, a single idealised Lewis structure is not an appropriate description for these transition states, which is typical in systems with extensive electron delocalisation. An alternative estimation of stabilisation energies may be instead gained by deleting a Fock matrix element that corresponds to a specific donor-acceptor interaction, whilst leaving other interactions the same, diagonalising the deleted Fock matrix and re-evaluating the total energy of this new density.[52] The stabilisation (deletion) energy is thus the difference between the total energies before and after matrix-element deletion. This analysis reveals that, generally, the strength of both the primary and secondary interactions changes simultaneously between reactions, and that the reactions with higher barriers have stronger $\pi_{C=C} - p^{+}_{Ch}$ interactions, suggesting greater electron movement between partially filled and partially vacant orbitals (**Table 3**). Contrary to initial expectations, the telluriranium ion reactions, which involve a 'softer' tellurium atom with more nucleophilic lone pairs, do not have stronger $\pi_{C=C} - p^{+}_{Ch}$ or n_{Ch}- $\pi^{*}_{C=C}$ interactions than the alternative

thiiranium ion reactions, which involve a 'harder' sulphur atom with more tightly bound lone pairs. This suggests that the orbital overlap must be significantly reduced in the former case leading to less electron delocalisation and hence smaller NBO interactions. This is reflected in the off-diagonal NBO Fock matrix element, $F_{(i,j)}$, values (**Table 3**), which are representative of the extent of orbital overlap and correlate with the trend in bond lengths discussed above (**Table 2**). For all of the identity reactions (**A**, **B** and **C**), the NBO interactions between the chalcogen and either alkene are very similar (**Table 3**). However, for the non-identity reaction **D**, there is a shift in the relative ordering of the interactions with the cyclohexyl moiety donating less (55.3 kcal mol^{-1}) into the p^{+}_{S} orbital than the styryl moiety (57.4 kcal mol^{-1}), approximately the same for the p^{+}_{Se} orbital, and then significantly more for the former (59.1 kcal mol^{-1}) into the p^{+}_{Te} orbital than the styryl moiety (33.0 kcal mol^{-1}). This trend is also observable in the back-bonding interaction and reflects the exoergicity of the reaction, with the Hammond postulate suggesting the structure of the sulphur transition state **27b** will be the most similar to the corresponding association complex **27a** ($\pi_{C=C}$ styrene – p^{+}_{S} > $\pi_{C=C}$ cyclohexene – p^{+}_{S}) as it is the most exoergic of reactions **D1-3** (**Figure 3**).

The nucleus-independent chemical shift (NICS) is an established method that provides a localised examination of magnetic shielding due to electron delocalisation with large negative NICS values often indicating aromaticity.[53] Despite a study by Wang *et al.* on the π-aromaticity of ground state three-membered ring systems suggesting that the dissected $NICS(0)_{\pi zz}$ value is a suitable indicator (as σ electrons dominate the magnetic shielding of the more convenient $NICS(1)_{zz}$ value),[54] there is the potential of contaminated π orbitals from ring substituents of the transition states in this study as the system is not fully planar.[55] In addition, the ring current is across two dual three-membered rings and NICS has been shown to provide misleading results with polyaromatic hydrocarbons (e.g. anthracene) as it only describes the local ring, not the conjugated system.[56] Though several studies have provided corrections for this by, for example, using an additive approach of a NICS-*XY*-scan of the $NICS_{\pi zz}$ values of the subunits of polyacenes,[57] these methods are not applicable to the π-ligand exchange transition states as they cannot be broken down into small units with their own ring currents. Thus, other measures of the magnetic properties as indicators of aromaticity in these transition states have been applied.

The anisotropy of the induced current density (ACID) has been used to discriminate between coarctate and pseudocoarctate reactions (as well as pericyclic and pseudopericyclic reactions) by determining the critical isosurface value (CIV).[30,58] The CIV is the point at which there is a disconnection at a critical point in the ACID scalar field isosurface. If the CIV < 0.02, then the reaction is considered pseudocoarctate reflecting weak electron delocalisation, whilst if the CIV is > 0.03 then the reaction is considered to be coarctate reflecting greater electron delocalisation,[59] generally attributed to aromaticity. Borderline cases occur if the 0.02 < CIV < 0.03, though Young *et al* have identified a reaction as pseudocoarctate despite a high CIV of 0.044,[59] so these values must be taken into consideration with other criteria as explained. Nevertheless, all reactions studied show CIVs < 0.02 as shown in **Table 4**, suggesting that all are pseudocoarctate, which supports the evidence thus far pointing to shifts in aromaticity as a minimal driving factor in these reactions. The split in CIV for reaction **D3** is due to the tellurium-cyclohexyl bonds having a slightly higher CIV (0.013) than the tellurium-styryl bonds (0.011) reflecting the different strengths in the NBO interactions. All reaction sets present no discernible trend between reaction barrier and the CIV with reactions **A** and **B** increasing in CIV down the group, but reactions **C** and **D** decreasing in CIV down the group. This may be related to the change in alkenes exchanging at the chalcogen, however, all the reactions being pseudocoarctate is the main conclusion from this set of data.

The ACID analysis of transition state **15b** from reaction **B3** has been provided in detail as an example of the pseudocoarctate nature of these π-ligand exchange reactions (**Figure 7**). The disconnection in the electron delocalisation occurs at a low CIV of 0.015 and occurs simultaneously between the tellurium

and all four ethene carbons reflecting the concomitant bond breaking and forming at one centre characteristic of a pseudocoarctate reaction. The isosurface alone gives information about the magnitude of the electron delocalisation in the system, but not the direction of the current. Hence, current density vectors were plotted on the isosurface and show a diatropic (clockwise) ring current relative to the applied magnetic field. The ACID analysis supports a borderline non-aromatic/weakly aromatic transition state, characteristic of a pseudocoarctate nature, but not an anti-aromatic nor strongly aromatic system.

The anisotropy of the magnetic susceptibility was used to analyse changes in the magnetic properties along the reaction coordinate. The advantage of examining the anisotropy rather than the total magnetic susceptibility is that it takes the difference between the larger component perpendicular to the ring plane and the smaller components parallel to the ring plane (χ_{anis} is also known as $\Delta\chi$ in the literature),[58] similar to the $NICS_{zz}$ concept, and is hence a more accurate measure of aromaticity. Various studies by Rodriguez-Otero *et al.* have found that large negative magnetic susceptibility anisotropies accompany aromatic pericyclic transition state species, and that pseudopericyclic transition states (and pseudocoarctate in one study) exhibit either little change, or at most a slight maximum in χ_{anis}, along the reaction path relative to the reactants.[60-63] Reactions **A1-3** and **C3** were chosen to investigate whether this held across a variety of reactions with different barrier heights (**A1-3**), and a barrierless reaction (**C3**). The non-identity reaction **D2** was also considered for analysis, but magnetic susceptibility calculations are global measures of aromaticity and may be influenced by structural moieties that are not of interest (such as the two phenyl rings present in **D2**), thus giving misleading results. Identity reactions **A1-3** show a slight maximum at the transition state (**A**, **Figure 8**), supporting the lack of aromaticity in these transition states and hence their pseudocoarctate nature. There is little change in the anisotropy of the magnetic susceptibility along the reaction coordinate for **C3** compared to the complex and this is not surprising given the structural and orbital similarity between the complex and transition state (**C3**, **Figure 8**), leading to the near barrierless reaction as mentioned previously.[26]

A first principles approach may be taken to discriminate between coarctate and pseudocoarctate TS by considering Lemal's definition of pseudopericyclic transition states in which "non-bonding and bonding atomic orbitals interchange roles" meaning a "disconnection in the cyclic array of overlapping orbitals".[64] **Figure 9** shows the significant $\pi_{C=C}$ - p^{+}_{Ch} and n_{Ch} - $\pi^{*}_{C=C}$ NBO interactions in TS **31b** and, as hinted at earlier in **Figure 1**, the vacant p^{+} orbital and the lone pair on the sulphur atom are orthogonal to one another leading to a disconnection in the orbital array at the central chalcogen. The first part of the above definition is more discerning as the chalcogen lone pair that interacts with the π* orbitals of the alkenes at the transition state is liberated from one of the σ_{Ch-C} orbitals of the initial iranium ion. NBO analysis along the reaction coordinate supports this as it shows that, though there is one lone pair available on the chalcogen from reactant to product (it is *anti* to the S-H bond), the lone pair interacting at the transition state only appears when the σ_{Ch-C} bonds are broken (evident from detection of the natural hybrid orbital's (NHO) polar and azimuthal angles of the lone pair) . The points along the pathway at which this interchange from bonding to non-bonding orbitals occurs for reactions **A1-3**, **C3** and **D2** are collated in **Tables S4-8** with the bond breaking occurring earlier for those reactions with lower barriers (such as **A3**). Thus, it is likely that every associative π-ligand exchange reaction of a chalcogen iranium ion is pseudocoarctate regardless of the nature of the central moiety or the alkenes it is being exchanged between.

Conclusion

The nature of the mechanism of π-ligand exchange reactions of chalcogen iranium ions has been explored comprehensively by DFT calculations based on previous computational and experimental work. Exploration of these reactions revealed not only the electrophilicity of the chalcogen as a reactivity factor, but also the overall strain in the iranium ions both in the reactants and products. The

initial association complex's similarity to the transition state was also observed to be a continual indicator of reactivity with lower barriers predicted, if not barrierless altogether, the greater the similarity. The NBO analysis supported earlier suggestions of two key interactions at the transition state involving two primary $\pi_{C=C}$ - p^{+}_{Ch} and one secondary n_{Ch} - $\pi^{*}_{C=C}$ leading to a Hückel number of delocalised π electrons. Based on these interactions and the previous experimental work, the π-ligand exchange reactions must be considered diagnostic of the iranium ion structure (rather than isomeric onium ions). The same conclusion has been made by Heck *et al.* for chloriranium and bromiranium ions (referred to as cyclic ethylenehalonium ions) for the transfer of a halogen moiety between alkenes.[65] The nature of these reactions was suggested to be pseudocoarctate (non-aromatic/weakly aromatic) rather than coarctate (aromatic) by analysis of the magnetic properties both at the transition state (ACID) and along the reaction coordinate (χ_{anis}). Further NBO analysis along the reaction coordinate supported Lemal's definition of pseudopericyclic transition states, which may be applied to pseudocoarctate transition states as well, with an interchange from bonding (σ_{Ch-C}) to non-bonding (n_{Ch}) orbitals during the reaction leading to disconnections in the orbital array. This work has also highlighted the fact that there are limited tools available to explore the magnetic properties of dual three-membered ring systems and may prompt further development in the field for understanding other transition states involving structural moieties outside of six- and five-membered rings.

Author Information

Corresponding Authors

*(S.C.B.) E-mail: brydons@student.unimelb.edu.au.

*(J.M.W.) E-mail: whitejm@unimelb.edu.au.

ORCID

Samuel C. Brydon: 0000-0002-8939-0249

Gabriel da Silva: 0000-0003-4284-4474

Jonathan M. White: 0000-0002-0707-6257

Conflicts of Interest

There are no conflicts to declare.

Acknowledgments

We thank the Australian Government for a Research Training Program (RTP) scholarship to S.B. The DFT calculations were performed on the Spartan High Performance Computing (HPC) System hosted by the Research Platform Services at the University of Melbourne.[66] Thanks to Fynn Roehricht from the Herges research group for help in setting up the ACID program. ACID calculations were conducted on the Argali HPC Service provided by the Melbourne School of Engineering hosted at the University of Melbourne.

Notes and References

1. Mueller, W. H. *Angew Chem Int Ed Eng* **1969**, 8(7), 482-492.
2. Smit, V. A.; Zefirov, N. S.; Bodrikov, I. V.; Krimer, M. Z. *Acc Chem Res* **1979**, 12(8), 282-288.
3. Modena, G.; Pasquato, L.; Lucchini, V. *Phosphorus, Sulfur, Silicon Relat Elem* **1994**, 95(1-4), 265-282.
4. Rayner, C. M. In Organosulfur Chemistry; Page, P., Ed.; Academic Press, 1995, p 89-131.
5. Danielle, M. B.; Thomas, W. *Curr Org Chem* **2006**, 10(15), 1893-1903.
6. Wirth, T. *Angew Chem Int Ed* **2000**, 39(21), 3740-3749.

7. Denmark, S. E.; Kalyani, D.; Collins, W. R. *J Am Chem Soc* **2010**, 132(44), 15752-15765.
8. Hartmann, E.; Denmark, S. E. *Helv Chim Acta* **2017**, 100(9), e1700158.
9. Denmark, S. E.; Hartmann, E.; Kornfilt, D. J. P.; Wang, H. *Nat Chem* **2014**, 6(12), 1056-1064.
10. Poleschner, H.; Seppelt, K. *Eur J Chem* **2018**, 24(64), 17155-17161.
11. Bock, J.; Daniliuc, C. G.; Bergander, K.; Mück-Lichtenfeld, C.; Hennecke, U. *Org Biomol Chem* **2019**, 17(12), 3181-3185.
12. Denmark, S. E.; Collins, W. R.; Cullen, M. D. *J Am Chem Soc* **2009**, 131(10), 3490-3492.
13. Smit, W. A.; Krimer, M. Z.; Vorob'eva, E. A. *Tetrahedron Lett* **1975**, 16(29), 2451-2454.
14. Capon, B. *Q Rev Chem Soc* **1964**, 18(1), 45-111.
15. Schmid, G. H.; Strukelj, M.; Dalipi, S. *Can J Chem* **1987**, 65(8), 1945-1950.
16. Denmark, S. E.; Vogler, T. *Eur J Chem* **2009**, 15(43), 11737-11745.
17. Denmark, S. E.; Kornfilt, D. J. P. *J Org Chem* **2017**, 82(6), 3192-3222.
18. Sølling, T. I.; Wild, S. B.; Radom, L. *Eur J Chem* **1999**, 5(2), 509-514.
19. Toshimitsu, A.; Nakano, K.; Mukai, T.; Tamao, K. *J Am Chem Soc* **1996**, 118(11), 2756-2757.
20. Toshimitsu, A.; Ito, M.; Uemura, S. *J Chem Soc, Chem Commun* **1989**(9), 530-531.
21. Toshimitsu, A. *Phosphorus, Sulfur, Silicon Relat Elem* **2005**, 180(3-4), 935-937.
22. Maji, B. *Adv Synth Catal* **2019**, 361(15), 3453-3489.
23. Ascheberg, C.; Bock, J.; Buß, F.; Mück-Lichtenfeld, C.; Daniliuc, C. G.; Bergander, K.; Dielmann, F.; Hennecke, U. *Eur J Chem* **2017**, 23(48), 11578-11586.
24. Lim, S. F.; Harris, B. L.; Khairallah, G. N.; Bieske, E. J.; Maître, P.; da Silva, G.; Adamson, B. D.; Scholz, M. S.; Coughlan, N. J. A.; O'Hair, R. A. J.; Rathjen, M.; Stares, D.; White, J. M. *J Org Chem* **2017**, 82(12), 6289-6297.
25. Brydon, S. C.; Lim, S. F.; Khairallah, G. N.; Maître, P.; Loire, E.; da Silva, G.; O'Hair, R. A. J.; White, J. M. *J Org Chem* **2019**, 84(16), 10076-10087.
26. Brydon, S. C.; Ren, Z.; da Silva, G.; Lim, S. F.; Khairallah, G. N.; Rathjen, M. J.; White, J. M.; O'Hair, R. A. J. *J Phys Chem A* **2019**, 123(38), 8200-8207.
27. Ortgies, S.; Breder, A. *ACS Catal* **2017**, 7(9), 5828-5840.
28. Herges, R. *J Chem Inf Model* **1994**, 34(1), 91-102.
29. Herges, R. *Angew Chem Int Ed Eng* **1994**, 33(3), 255-276.
30. Herges, R. *J Org Chem* **2015**, 80(23), 11869-11876.
31. Frisch, M.J.; Trucks, G.W.; Schlegel, H.B.; Scuseria, G. E.; Robb, M. A.; Cheeseman, J. R.; Scalmani, G.; Barone, V.; Petersson, G. A.; Nakatsuji, H.; et al. Gaussian Revision B.01; Gaussian, Inc., Wallingford CT, 2016.
32. Zhao, Y.; Truhlar, D. G. *Theor Chem Acc* **2008**, 120(1), 215-241.
33. Weigend, F.; Ahlrichs, R. *Phys Chem Chem Phys* **2005**, 7(18), 3297-3305.
34. Mardirossian, N.; Head-Gordon, M. *Mol Phys* **2017**, 115(19), 2315-2372.
35. Zhao, Y.; Truhlar, D. G. *J Org Chem* **2007**, 72(1), 295-298.
36. Dau, P. D.; Armentrout, P. B.; Michelini, M. C.; Gibson, J. K. *Phys Chem Chem Phys* **2016**, 18(10), 7334-7340.
37. Glendening, E. D.; Badenhoop, J, K.; Reed, A. E.; Carpenter, J. E.; Bohmann, J. A.; Morales, C. M.; Karafiloglou, P; Landis, C. R.; Weinhold, F. NBO 7.0. Theoretical Chemistry Institute, University of Wisconsin, Madison, 2018.
38. Hanwell, M. D.; Curtis, D. E.; Lonie, D. C.; Vandermeersch, T.; Zurek, E.; Hutchison, G. R. *J Cheminformatics* **2012**, 4(1), 17.
39. Weinhold, F.; Landis, C. R.; Glendening, E. D. *Int Rev Phys Chem* **2016**, 35(3), 399-440.
40. Keith, T. A.; Bader, R. F. W. *Chem Phys Lett* **1992**, 194(1), 1-8.
41. Geuenich, D.; Hess, K.; Köhler, F.; Herges, R. *Chem Rev* **2005**, 105(10), 3758-3772.
42. Keith, T. A.; Bader, R. F. W. *Chem Phys Lett* **1993**, 210(1), 223-231.
43. IUPAC Gold Book, https://goldbook.iupac.org/terms/view/I02940, (accessed January, 2020).
44. Brauman, J. I. *J Mass Spectrom* **1995**, 30(12), 1649-1651.

45. Glukhovtsev, M. N.; Pross, b. A.; Radom, L. *J Am Chem Soc* **1995**, 117(7), 2024-2032.
46. Wladkowski, B. D.; Brauman, J. I. *J Phys Chem* **1993**, 97(50), 13158-13164.
47. Schwabe, T.; Grimme, S. *J Phys Chem A* **2009**, 113(13), 3005-3008.
48. Zheng, J.; Zhao, Y.; Truhlar, D. G. *J Chem Theory Comput* **2009**, 5(4), 808-821.
49. Birney, D. M. *J Am Chem Soc* **2000**, 122(44), 10917-10925.
50. Birney, D. M. *J Org Chem* **1996**, 61(1), 243-251.
51. Zhou, C.; Birney, D. M. *J Am Chem Soc* **2002**, 124(18), 5231-5241.
52. Carpenter, J. E.; Weinhold, F. *J Mol Struc Theochem* **1988**, 169, 41-62.
53. Chen, Z.; Wannere, C. S.; Corminboeuf, C.; Puchta, R.; Schleyer, P. v. R. *Chem Rev* **2005**, 105(10), 3842-3888.
54. Wang, H.-J.; Schleyer, P. v. R.; Wu, J. I.; Wang, Y.; Wang, H.-J. *Int J Quantum Chem* **2011**, 111(5), 1031-1038.
55. Gershoni-Poranne, R.; Stanger, A. *Chem Soc Rev* **2015**, 44(18), 6597-6615.
56. Bultinck, P. *Faraday Discuss* **2007**, 135(0), 347-365.
57. Gershoni-Poranne, R. *Eur J Chem* **2018**, 24(16), 4165-4172.
58. Herges, R. In The Chemical Bond; Shaik, G. F. a. S., Ed., 2014, p 383-420.
59. Young, B. S.; Herges, R.; Haley, M. M. *Chem Commun* **2012**, 48(76), 9441-9455.
60. Cabaleiro-Lago, E. M.; Rodríguez-Otero, J.; García-López, R. M.; Peña-Gallego, A.; Hermida-Ramón, J. M. *Eur J Chem* **2005**, 11(20), 5966-5974.
61. Rodríguez-Otero, J.; Cabaleiro-Lago, E. M. *Angew Chem Int Ed* **2002**, 41(7), 1147-1150.
62. Peña-Gallego, A.; Rodríguez-Otero, J.; Cabaleiro-Lago, E. M. *Eur J Org Chem* **2005**, 2005(15), 3228-3232.
63. Rodríguez-Otero, J.; Cabaleiro-Lago, E. M. *Eur J Chem* **2003**, 9(8), 1837-1843.
64. Ross, J. A.; Seiders, R. P.; Lemal, D. M. *J Am Chem Soc* **1976**, 98(14), 4325-4327.
65. Heck, A. J. R.; de Koning, L. J.; Nibbering, N. M. M. *Org Mass Spectrom* **1993**, 28(3), 235-244.
66. Lafayette, L.; Sauter, G.; Vu, L.; Meade, B. Spartan Performance and Flexibility: An HPC-Cloud Chimera. Presented at the OpenStack Summit, Barcelona, October 27, 2016.

Table 1. Electronic energies of the complexes and transition states of identity reactions **A1-3**, **B1-3** and **C1-3** relative to the free reactants calculated at M06-2X/def2-TZVP compared to previous studies (in kJ mol^{-1}).

	This Study		Previous Studies		
Reaction	**Complex**	**Transition State**	**Association Complex**	**Transition State**	**Dissociation Complex**
A1*	-24.1	+48.2	-25.6	+46.6	-25.6
A2	-27.1	+6.8			
A3	-38.5	-32.7			
B1[#]	-17.2	+79.8	-17.2	+80.6	-15.3
B2[#]	-21.0	+29.2	-21.0	+30.0	-19.1
B3[#]	-30.0	-17.3	-30.0	-16.8	-28.7
C1[#]	-28.2	+34.0	-28.3	+33.3	-29.8
C2[#]	-32.0	-8.7	-32.1	-9.4	-33.4
C3[#]	-48.9	-48.9	-49.4	-49.6	-49.8

*Compared to those in reference 18 calculated at G2 (ZPE = MP2) on optimised MP2(full)/6-31G(d) geometries. [#]Compared to those partially deuterated systems in reference 26 calculated at M06-2X/def2-TZVP on geometries optimised at the same level. Blank spaces are for those with no prior study.

Table 2. Barrier heights relative to association complexes ($\Delta E^{\ddagger}_{RDS}$) and selected geometric parameters for the transition states of reactions **A**-**D**.

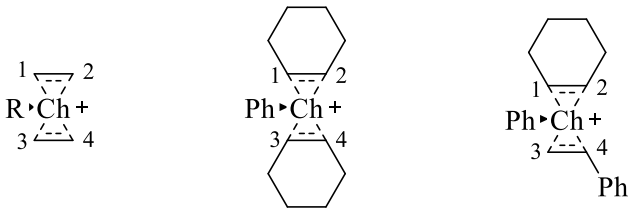

Reaction	$\Delta E^{\ddagger}_{RDS}$ *	MID#^	C_1-Ch-C_2^	C_3-Ch-C_4^	C_1-Ch&	C_2-Ch&	C_3-Ch&	C_4-Ch&
A1	+72.3	9.7	34.0	34.0	2.327	2.327	2.327	2.327
A2	+33.9	11.1	32.4	32.4	2.436	2.436	2.436	2.436
A3	+5.8	13.9	30.2	30.2	2.603	2.603	2.603	2.603
B1	+97.0	3.9	33.1	33.1	2.381	2.381	2.381	2.381
B2	+50.2	1.0	31.9	31.9	2.470	2.470	2.470	2.470
B3	+12.7	6.6	29.9	29.9	2.628	2.628	2.628	2.628
C1	+62.2	5.6	33.0	33.0	2.410	2.395	2.396	2.410
C2	+23.3	0.8	31.8	31.8	2.504	2.485	2.484	2.504
C3	+0.1	5.6	29.7	29.8	2.664	2.646	2.643	2.661
D1	+60.6	8.8	33.0	32.7	2.389	2.425	2.283	2.519
D2	+23.7	4.2	31.8	31.5	2.500	2.490	2.399	2.598
D3	+2.2	4.6	30.9	28.6	2.579	2.573	2.656	2.807

* $\Delta E^{\ddagger}_{RDS} = E^{\ddagger} - E_{\text{association complex}}$ in kJ mol^{-1} #Taken as the absolute difference between the angle of the midpoint of one C=C bond to the chalcogen to the other C=C bond, and 180°. ^ in degrees (°). & in angstrom (Å).

Table 3. Selected natural bond orbital interactions determined by deletions analysis (in kcal mol^{-1}).

Reaction	$\pi_{C1=C2} - p^{+}_{Ch}$		$\pi_{C3=C4} - p^{+}_{Ch}$		$n_{Ch} - \pi^{*}_{C1=C2}$		$n_{Ch} - \pi^{*}_{C3=C4}$	
	E_{DEL}	$F_{(i,j)}$	E_{DEL}	$F_{(i,j)}$	E_{DEL}	$F_{(i,j)}$	E_{DEL}	$F_{(i,j)}$
A1	73.3	0.170	73.3	0.170	19.8	0.091	19.8	0.091
A2	66.9	0.161	66.9	0.161	19.0	0.087	19.0	0.087
A3	53.8	0.146	53.9	0.146	16.7	0.078	16.7	0.078
B1	61.8	0.157	61.8	0.157	15.8	0.081	15.8	0.081
B2	59.3	0.153	59.3	0.153	16.7	0.081	16.7	0.081
B3	48.9	0.140	48.9	0.140	15.4	0.075	15.4	0.075
C1	57.9	0.151	57.8	0.150	12.8	0.076	12.8	0.076
C2	55.5	0.146	55.4	0.146	13.3	0.076	13.2	0.076
C3	44.6	0.132	45.0	0.133	11.8	0.069	12.0	0.069
D1	55.2	0.149	57.4	0.154	12.4	0.075	12.8	0.075
D2	54.6	0.147	54.1	0.146	13.0	0.074	13.0	0.075
D3	59.1	0.150	33.0	0.117	16.4	0.079	8.6	0.059

Table 4. Critical isosurface values (CIV) determined by anisotropy of the induced current density analysis for reactions **A**-**D**

REACTION	CIV	REACTION	CIV
A1	0.011	**C1**	0.014
A2	0.011	**C2**	0.012
A3	0.013	**C3**	0.011
B1	0.012	**D1**	0.016
B2	0.013	**D2**	0.013
B3	0.015	**D3**	0.013/0.011

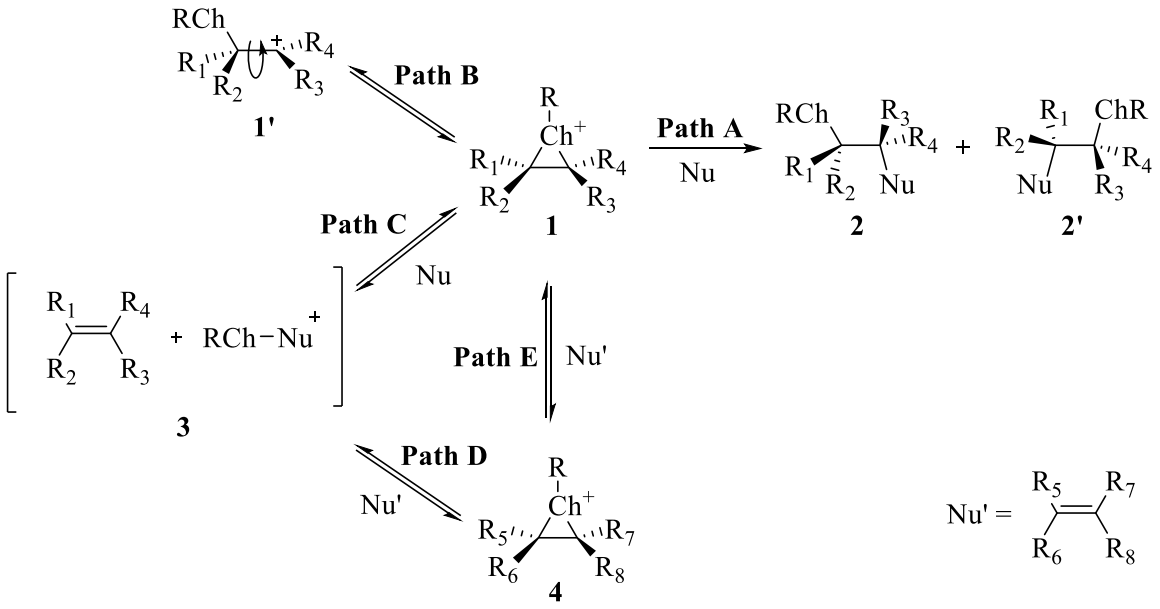

Scheme 1. Reaction and racemisation pathways of chalcogen (Ch = S, Se or Te) iranium ion **1** with nucleophiles (adapted from references 16 and 24)

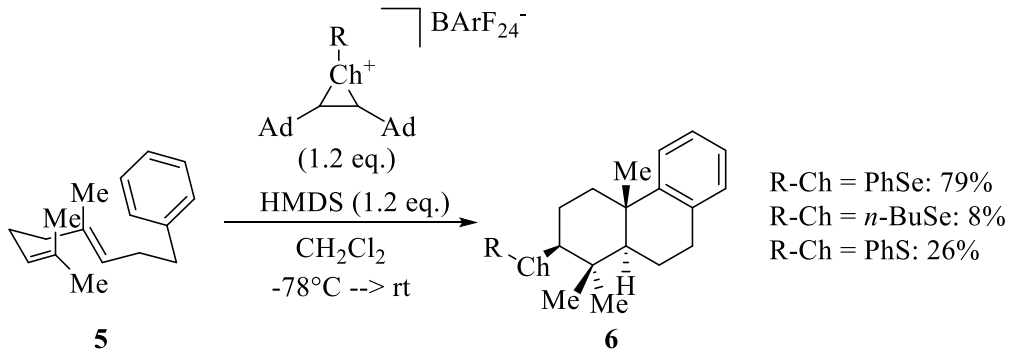

Scheme 2. Polyene type cyclisation of **5** to give tricyclic **6** induced by chalcogen iranium ions in the presence of non-coordinating counter ion tetrakis(3,5-bis(trifluoromethyl)phenyl)borate, $BArF_{24}^-$ (adapted from reference 11).

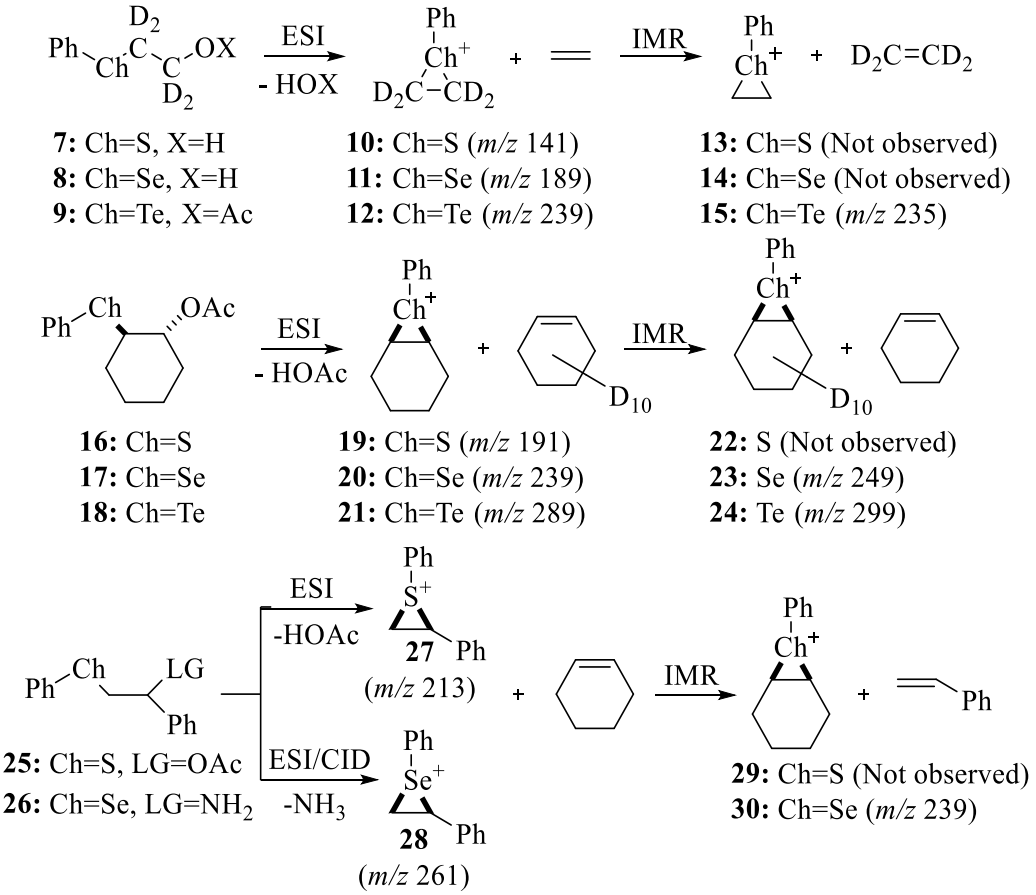

Scheme 3. Experimental π-ligand exchange reactions of chalcogen iranium ions **10-12**, **19-21** and **27-28** in the gas phase performed in a linear ion-trap quadrupole (LTQ) mass spectrometer (adapted from references 24-26). LG = leaving group.

Figure 1. Significant orbital interactions in the transition states of π-ligand exchange of chalcogen iranium ions (adapted from reference 18).

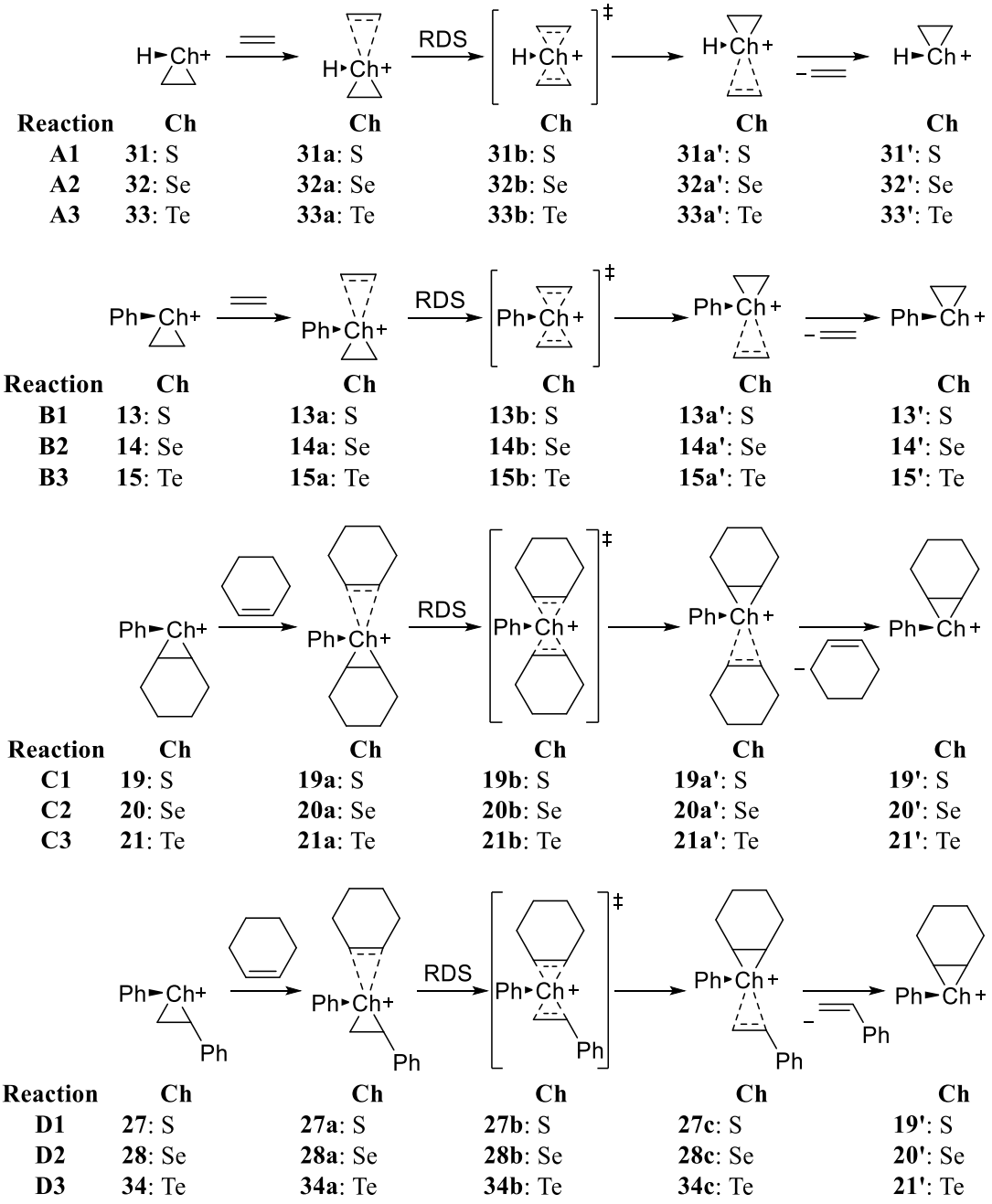

Reaction	Ch	Ch	Ch	Ch	Ch
A1	**31**: S	**31a**: S	**31b**: S	**31a'**: S	**31'**: S
A2	**32**: Se	**32a**: Se	**32b**: Se	**32a'**: Se	**32'**: Se
A3	**33**: Te	**33a**: Te	**33b**: Te	**33a'**: Te	**33'**: Te

Reaction	Ch	Ch	Ch	Ch	Ch
B1	**13**: S	**13a**: S	**13b**: S	**13a'**: S	**13'**: S
B2	**14**: Se	**14a**: Se	**14b**: Se	**14a'**: Se	**14'**: Se
B3	**15**: Te	**15a**: Te	**15b**: Te	**15a'**: Te	**15'**: Te

Reaction	Ch	Ch	Ch	Ch	Ch
C1	**19**: S	**19a**: S	**19b**: S	**19a'**: S	**19'**: S
C2	**20**: Se	**20a**: Se	**20b**: Se	**20a'**: Se	**20'**: Se
C3	**21**: Te	**21a**: Te	**21b**: Te	**21a'**: Te	**21'**: Te

Reaction	Ch	Ch	Ch	Ch	Ch
D1	**27**: S	**27a**: S	**27b**: S	**27c**: S	**19'**: S
D2	**28**: Se	**28a**: Se	**28b**: Se	**28c**: Se	**20'**: Se
D3	**34**: Te	**34a**: Te	**34b**: Te	**34c**: Te	**21'**: Te

Scheme 4. π-Ligand exchange identity (**A**, **B** and **C**) and non-identity (**D**) reactions of chalcogen iranium ions with the rate determining step (RDS) indicated (based on references 24-26).

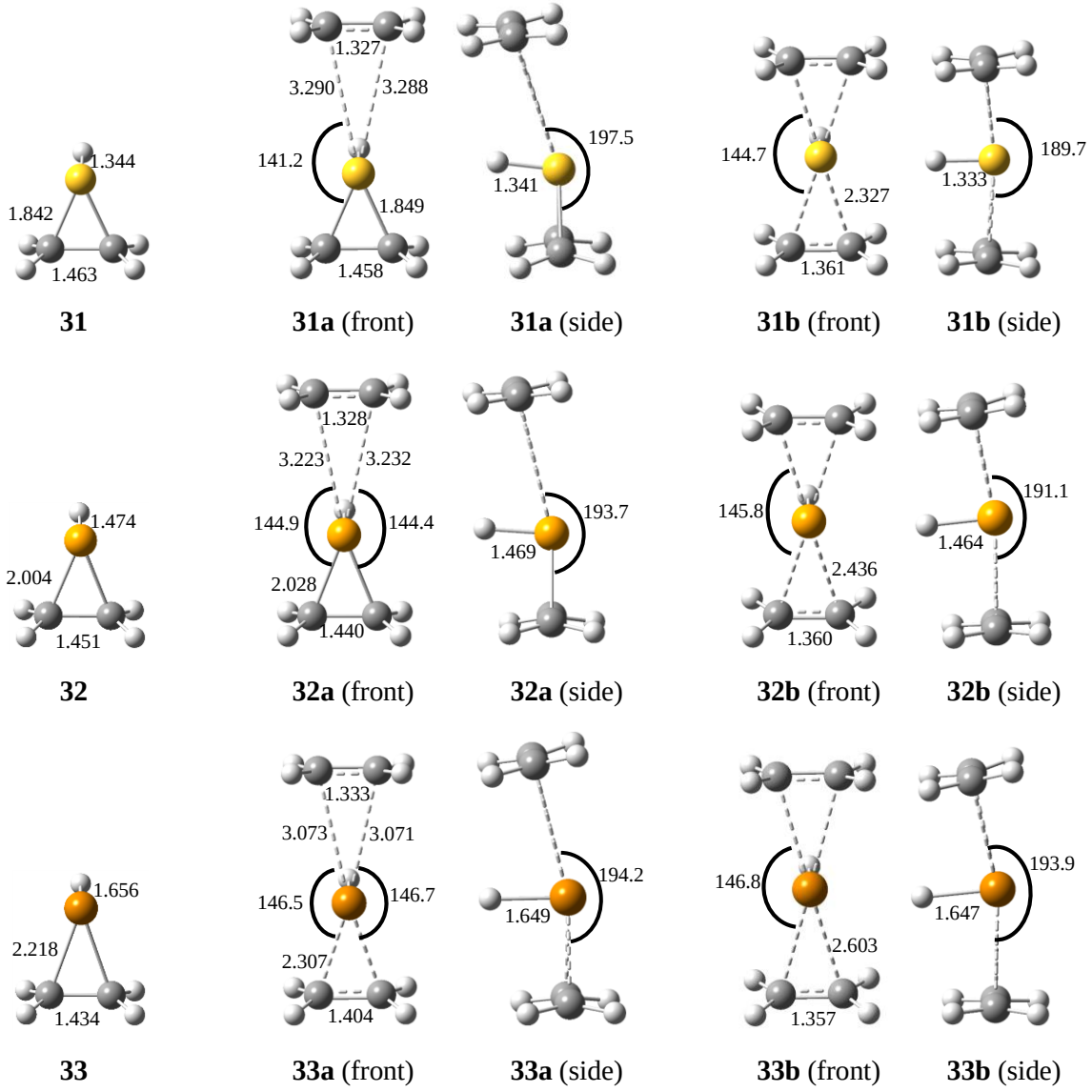

Figure 2. Calculated structures for key species in reactions **A1** (top), **A2** (middle) and **A3** (bottom). Bond lengths in angstrom (Å), angles in degrees (°). Due to symmetry, not all key bond lengths and angles are given if the same to the third or first decimal place respectively.

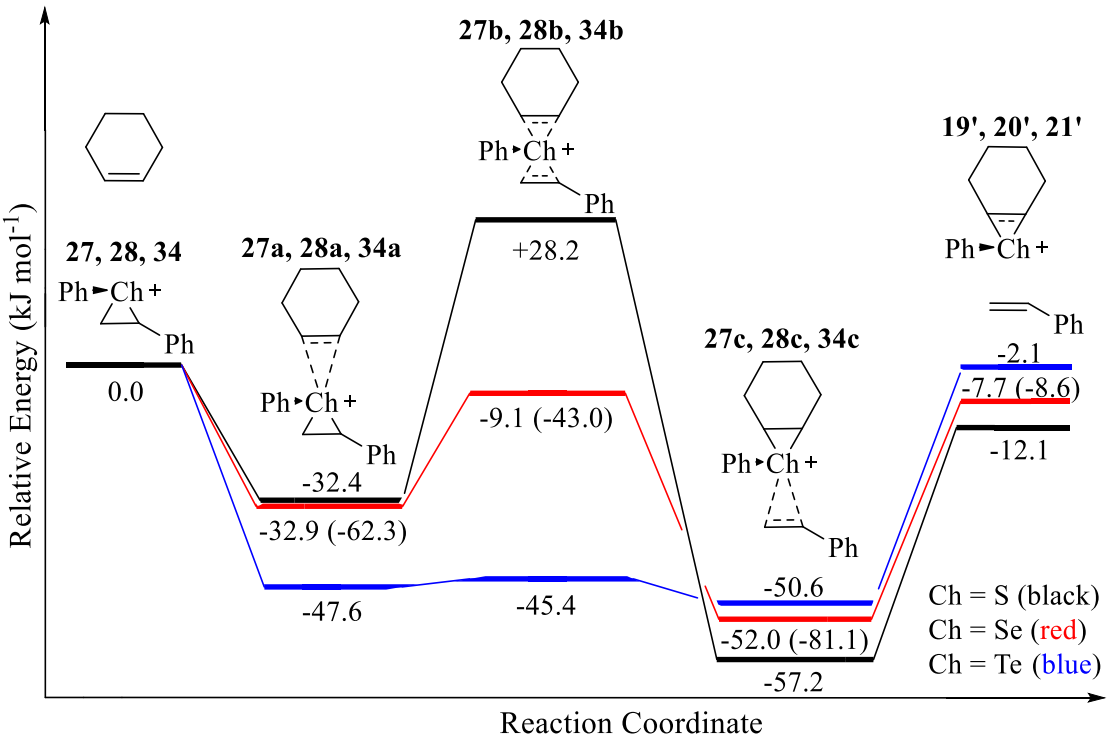

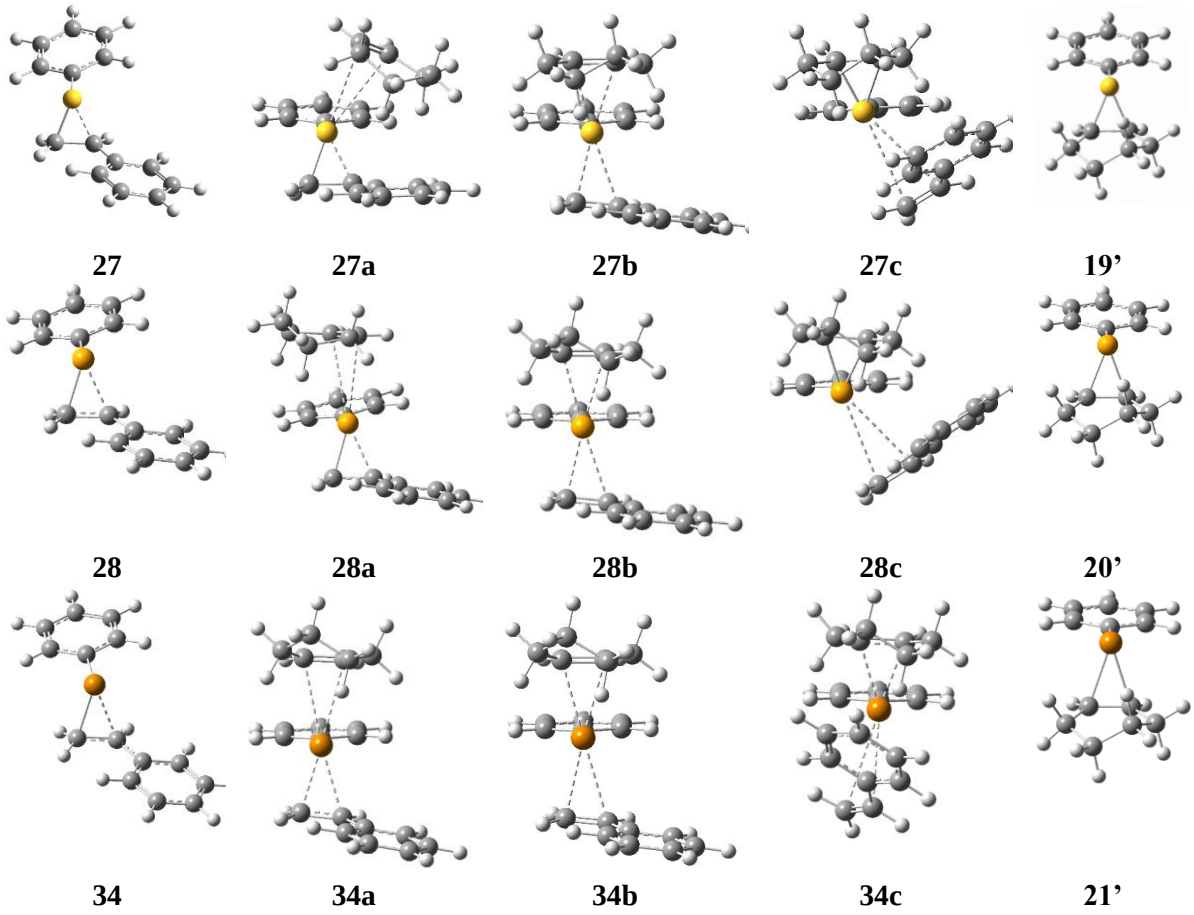

Figure 3. Relative energy diagram of **D1-3** π-ligand exchange reactions for chalcogen iranium ions **27** (adapted from reference 25), **28** and **34** with cyclohexene to afford products **19'-21'** (Ch = S – black; Se – red; Te – blue). Energies given as Δ*E* in kJ mol^{-1} at M06-2X/def2-TZVP relative to the free reactants. Energies in brackets correspond to previous study of Ch = Se calculated at M06/6-31+G(d), given as Δ*E* at 298 K in kJ mol^{-1}.[24]

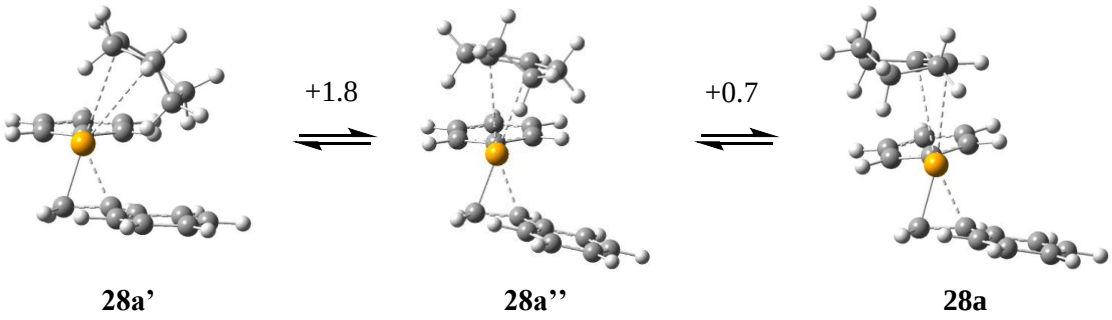

Scheme 5. Isomerisation of **28a'** to **28a** *via* transition state **28a''**. Energies given as Δ*E* in kJ mol^{-1} at M06-2X/def2-TZVP relative to **28a'**.

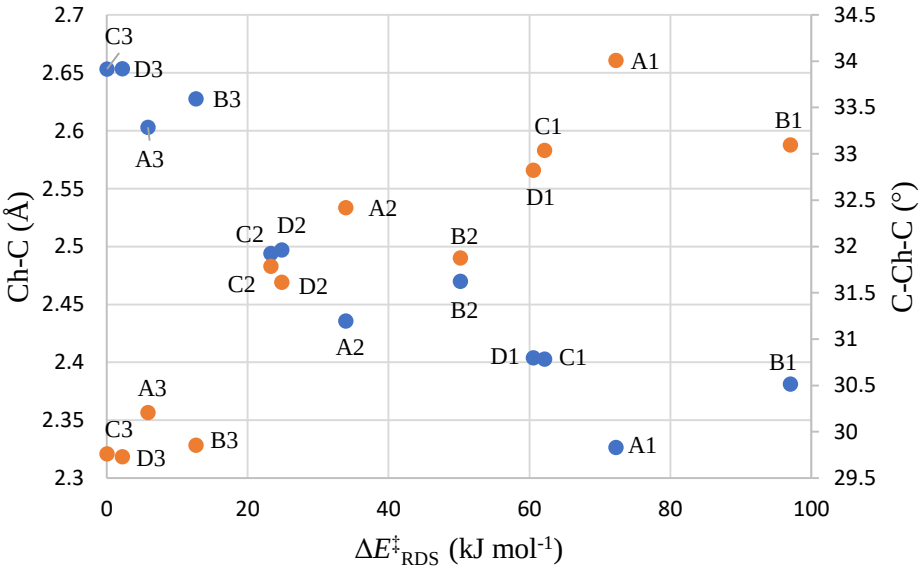

Figure 4. Plot of the average Ch-C bond length in Å (blue dots, $R^2 = 0.825$) and the average C-Ch-C angle in ° (orange dots, $R^2 = 0.808$) for transition states in reactions **A-D** against barrier height relative to association complex (kJ mol^{-1}).

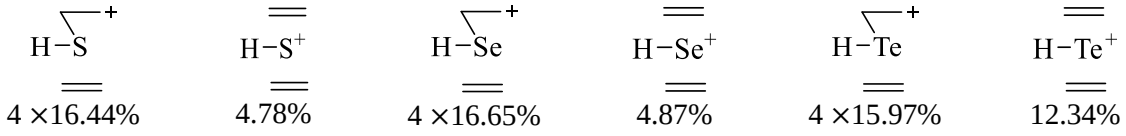

Figure 5. Selected Lewis structures from natural resonance theory analysis of transition states **31b-33b**

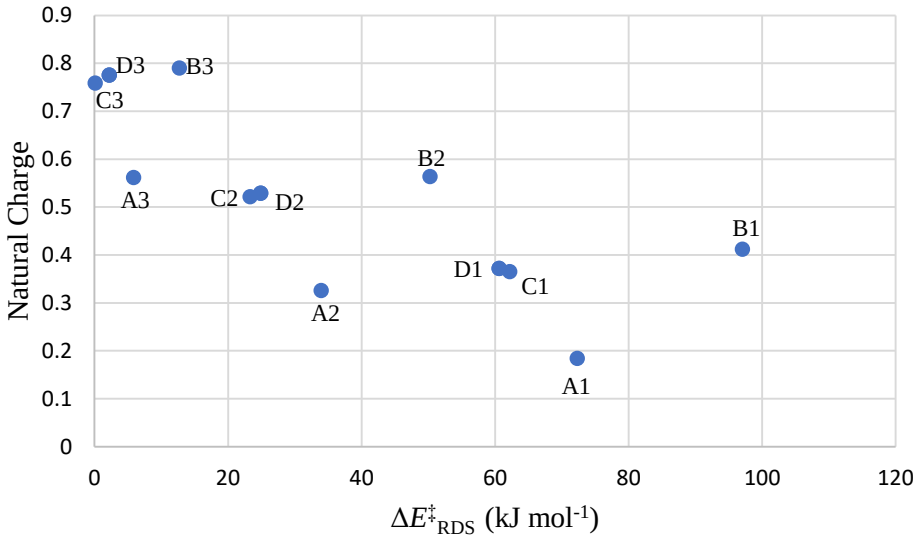

Figure 6. Plot of natural charge on the chalcogen for all transition states against barrier height relative to the association complex (kJ mol^{-1}) with $R^2 = 0.6318$.

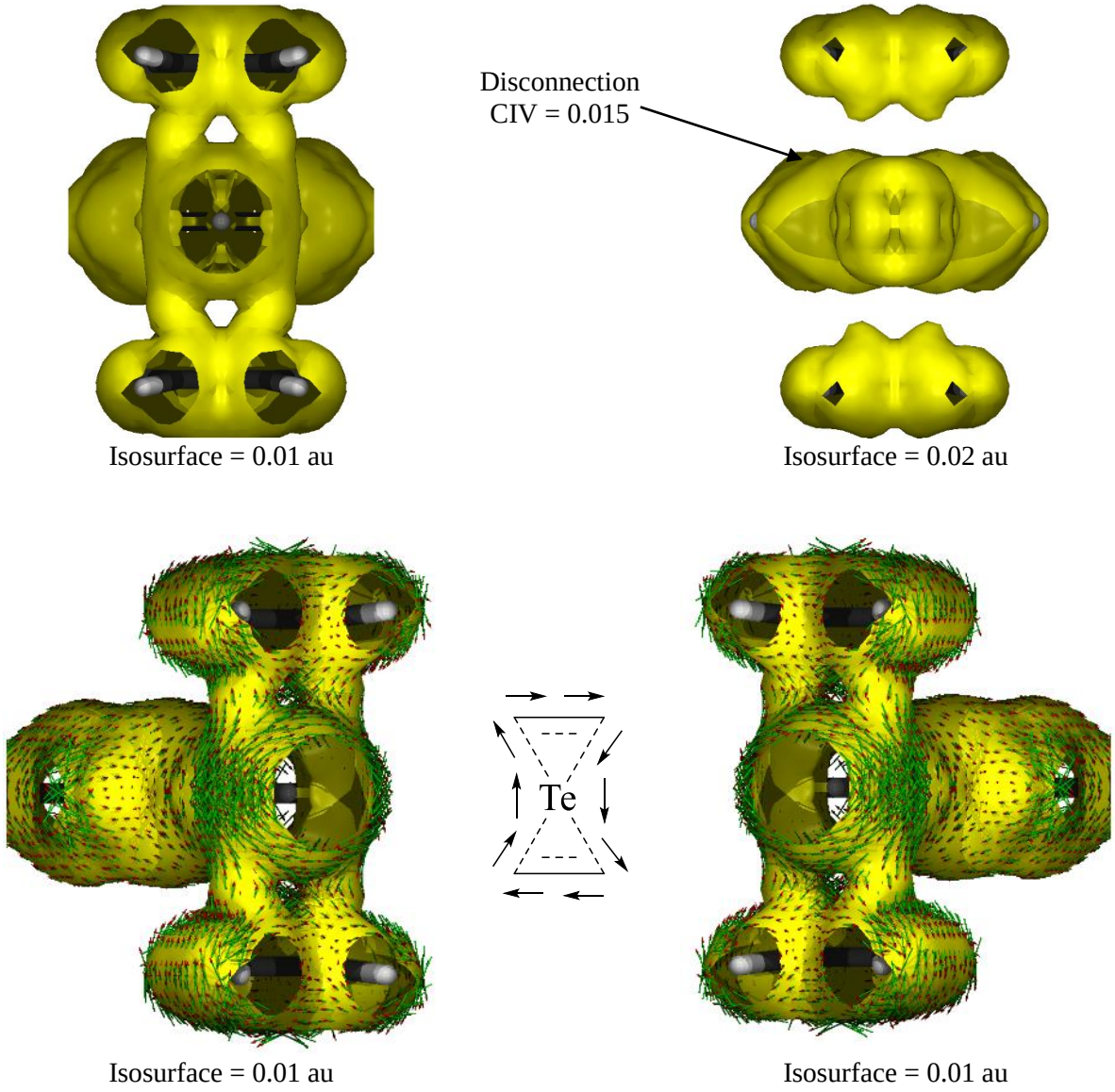

Figure 7. ACID plots at variable isosurface values of transition state **15b** from reaction **B3** involving the transfer of the $PhTe^+$ moiety between ethenes with all four of the bonds breaking/forming having a CIV value of 0.015 as indicated in the top structures. The current density vectors have been plotted on the two bottom structures to show the direction of the ring current (the right hand side has been rotated 180° around the $C{=}C_{mid}$ – Ch – $C{=}C_{mid}$ axis) with the diagram in the centre (the phenyl group points into the page and is omitted for clarity) representing the direction of electron flow as black arrows. The direction of the magnetic field lies along the Ph – Te axis pointing out of the page.

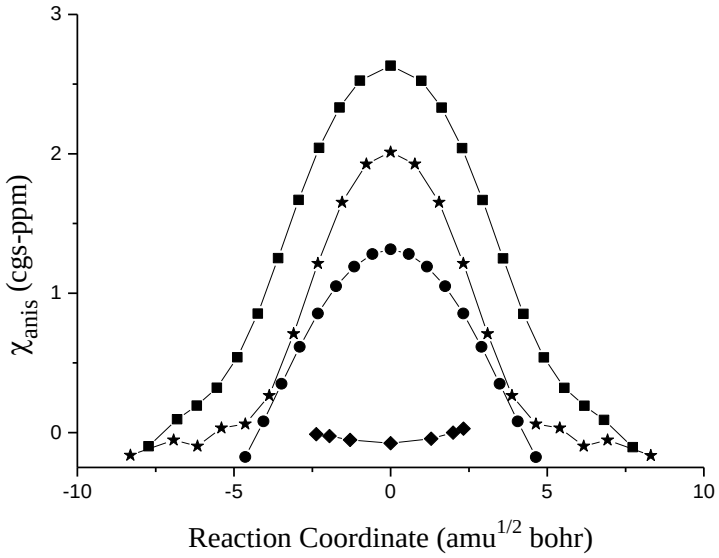

Figure 8. Change in the anisotropy of the magnetic susceptibility, χ_{anis}, (cgs-ppm) along the reaction coordinate (amu$^{1/2}$ bohr) of identity reactions **A1** (★), **A2** (■), **A3** (●) and **C3** (♦) relative to respective association complexes (raw data is collated in **Tables S4-7** in the Supporting information).

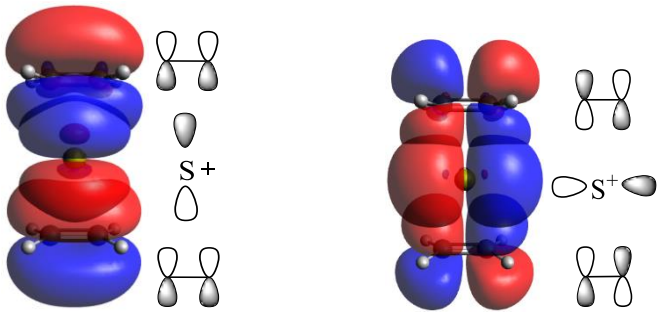

$2 \times \pi_{C=C}$ - p^{+}_{Ch} $\quad\quad$ n_{Ch} - $\pi^{*}_{C=C}$

Figure 9. Significant natural bond orbital interactions in the sulphur transition state **31b** visualised at an isosurface value of 0.02 au. Hydrogens have been excluded in the schematic orbitals for clarity.

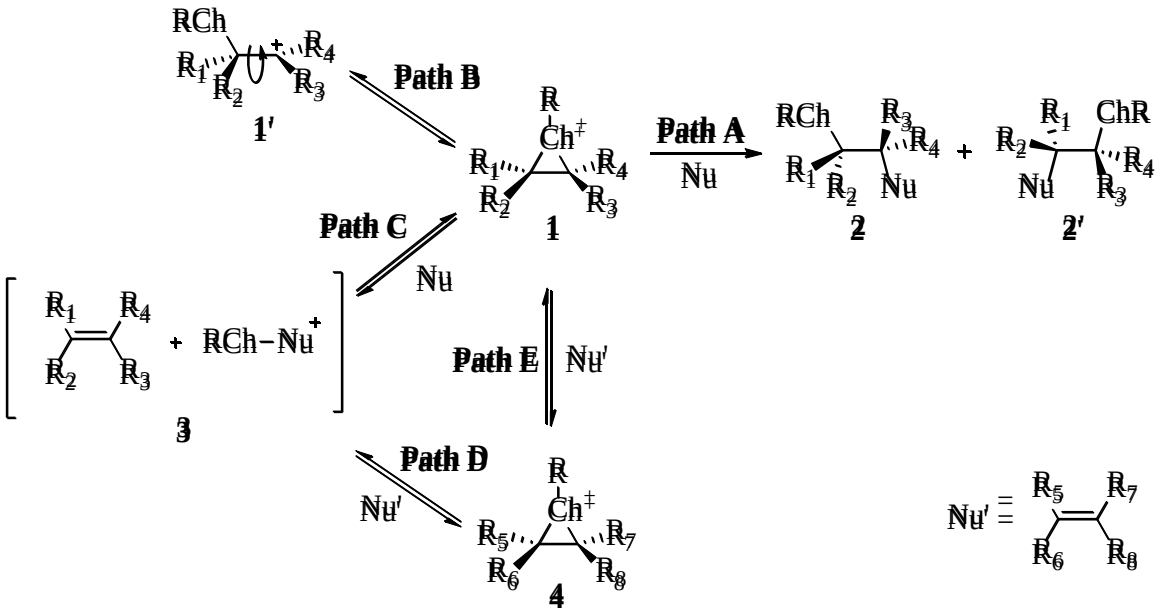

Scheme 1. Reaction and racemisation pathways of chalcogen (Ch = S, Se or Te) iranium ion **1** with nucleophiles (adapted from references 16 and 24)

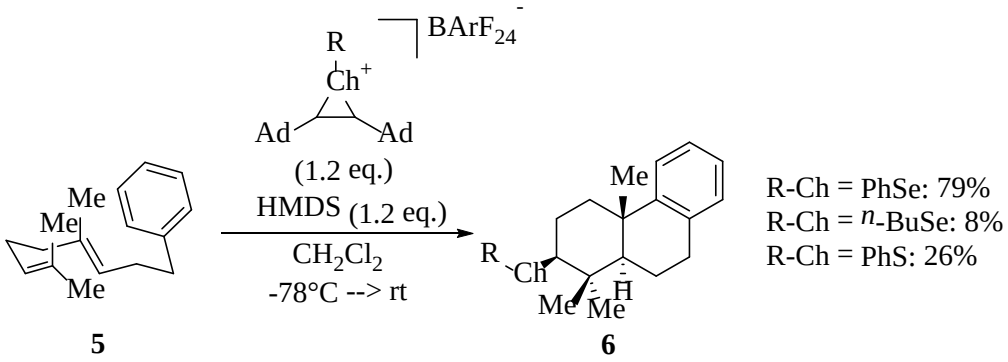

Scheme 2. Polyene type cyclisation of **5** to give tricyclic **6** induced by chalcogen iranium ions in the presence of non-coordinating counter ion tetrakis(3,5-bis(trifluoromethyl)phenyl)borate, $BArF_{24}^-$ (adapted from reference 11).

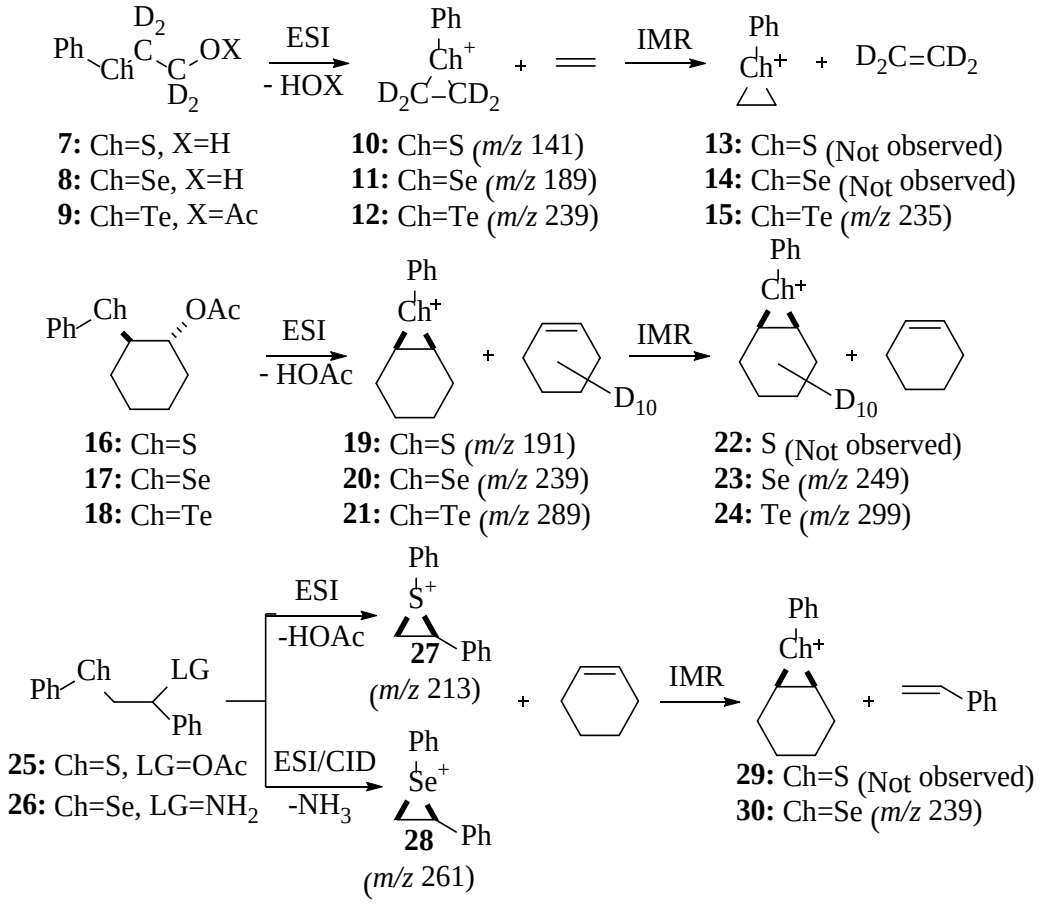

Scheme 3. Experimental π-ligand exchange reactions of chalcogen iranium ions **10-12**, **19-21** and **27-28** in the gas phase performed in a linear ion-trap quadrupole (LTQ) mass spectrometer (adapted from references 24-26). LG = leaving group.

Figure 1. Significant orbital interactions in the transition states of π-ligand exchange of chalcogen iranium ions (adapted from reference 18).

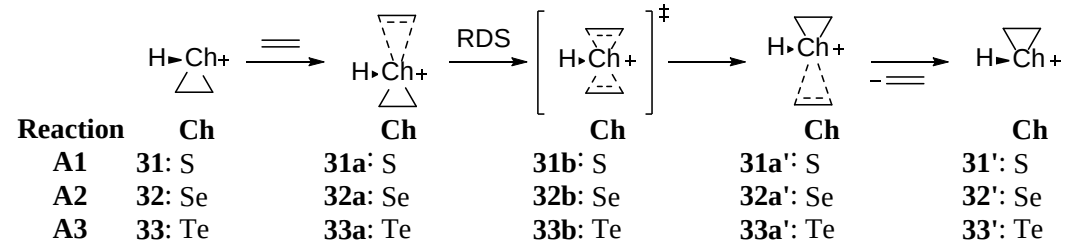

Reaction	Ch	Ch	Ch	Ch	Ch
A1	**31**: S	**31a**: S	**31b**: S	**31a'**: S	**31'**: S
A2	**32**: Se	**32a**: Se	**32b**: Se	**32a'**: Se	**32'**: Se
A3	**33**: Te	**33a**: Te	**33b**: Te	**33a'**: Te	**33'**: Te

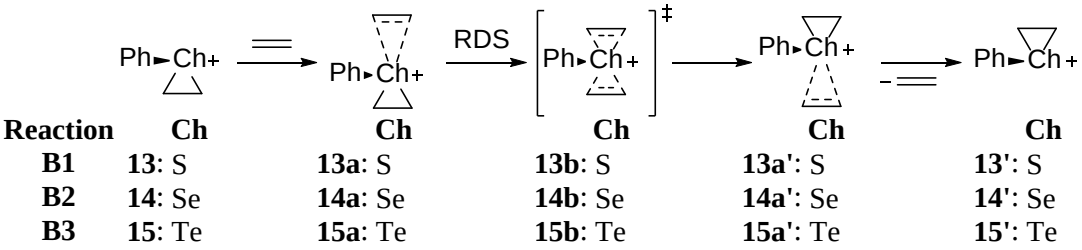

Reaction	Ch	Ch	Ch	Ch	Ch
B1	**13**: S	**13a**: S	**13b**: S	**13a'**: S	**13'**: S
B2	**14**: Se	**14a**: Se	**14b**: Se	**14a'**: Se	**14'**: Se
B3	**15**: Te	**15a**: Te	**15b**: Te	**15a'**: Te	**15'**: Te

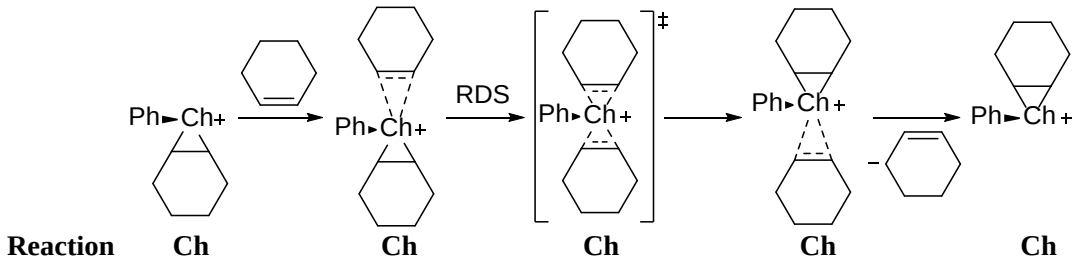

Reaction	Ch	Ch	Ch	Ch	Ch
C1	**19**: S	**19a**: S	**19b**: S	**19a'**: S	**19'**: S
C2	**20**: Se	**20a**: Se	**20b**: Se	**20a'**: Se	**20'**: Se
C3	**21**: Te	**21a**: Te	**21b**: Te	**21a'**: Te	**21'**: Te

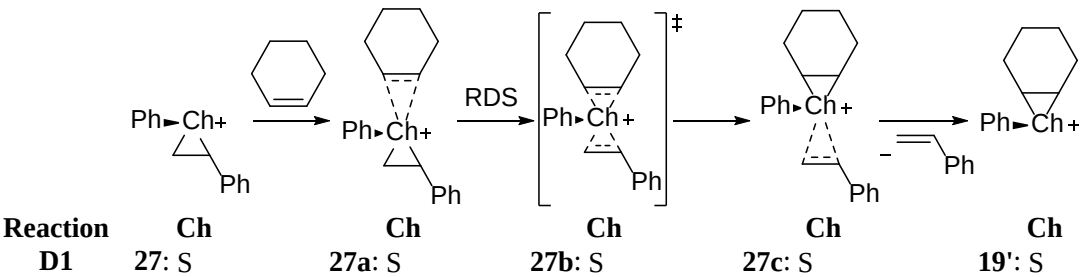

Reaction	Ch	Ch	Ch	Ch	Ch
D1	**27**: S	**27a**: S	**27b**: S	**27c**: S	**19'**: S
D2	**28**: Se	**28a**: Se	**28b**: Se	**28c**: Se	**20'**: Se
D3	**34**: Te	**34a**: Te	**34b**: Te	**34c**: Te	**21'**: Te

Scheme 4. π-Ligand exchange identity (**A**, **B** and **C**) and non-identity (**D**) reactions of chalcogen iranium ions with the rate determining step (RDS) indicated (based on references 24-26).

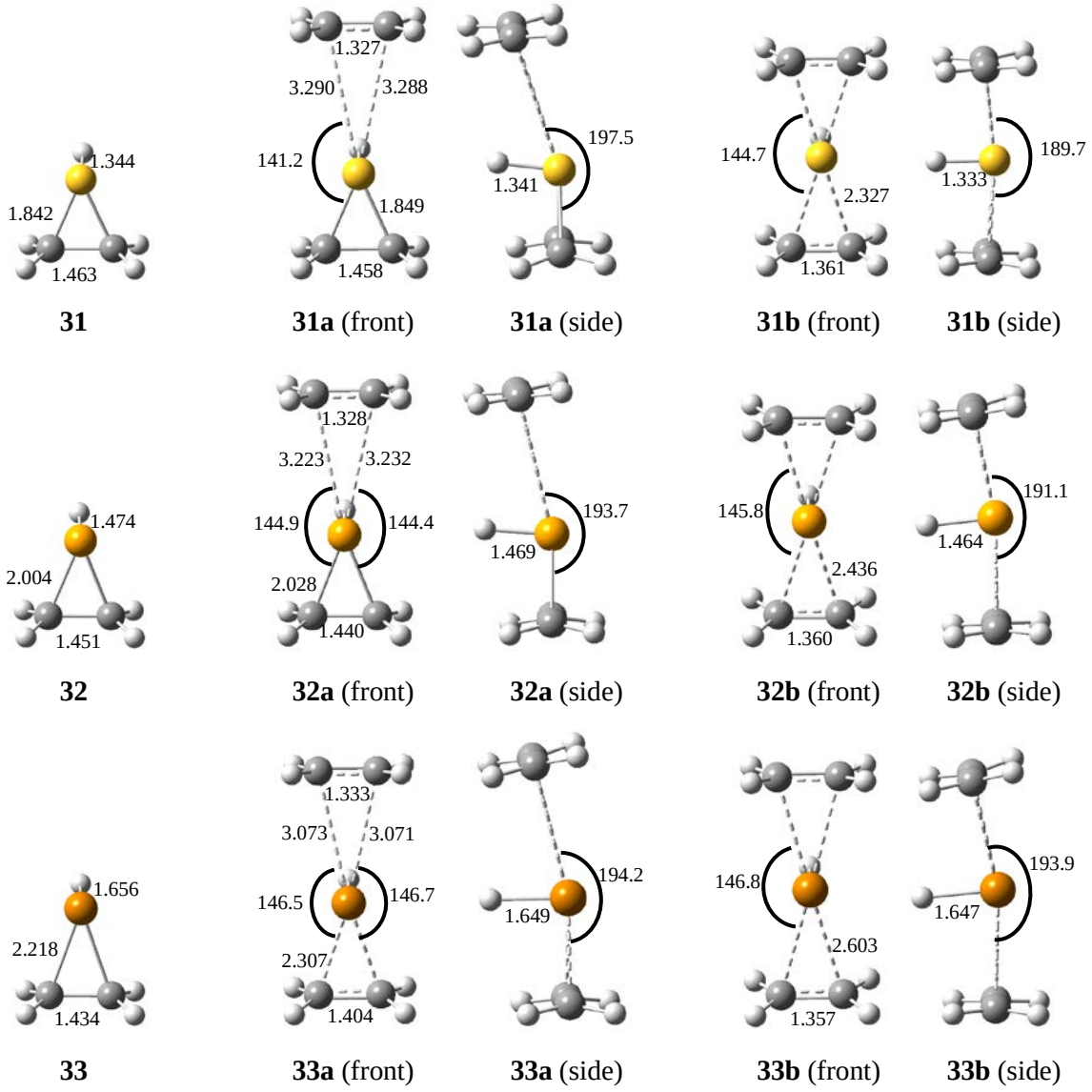

Figure 2. Calculated structures for key species in reactions **A1** (top), **A2** (middle) and **A3** (bottom). Bond lengths in angstrom (Å), angles in degrees (°). Due to symmetry, not all key bond lengths and angles are given if the same to the third or first decimal place respectively.

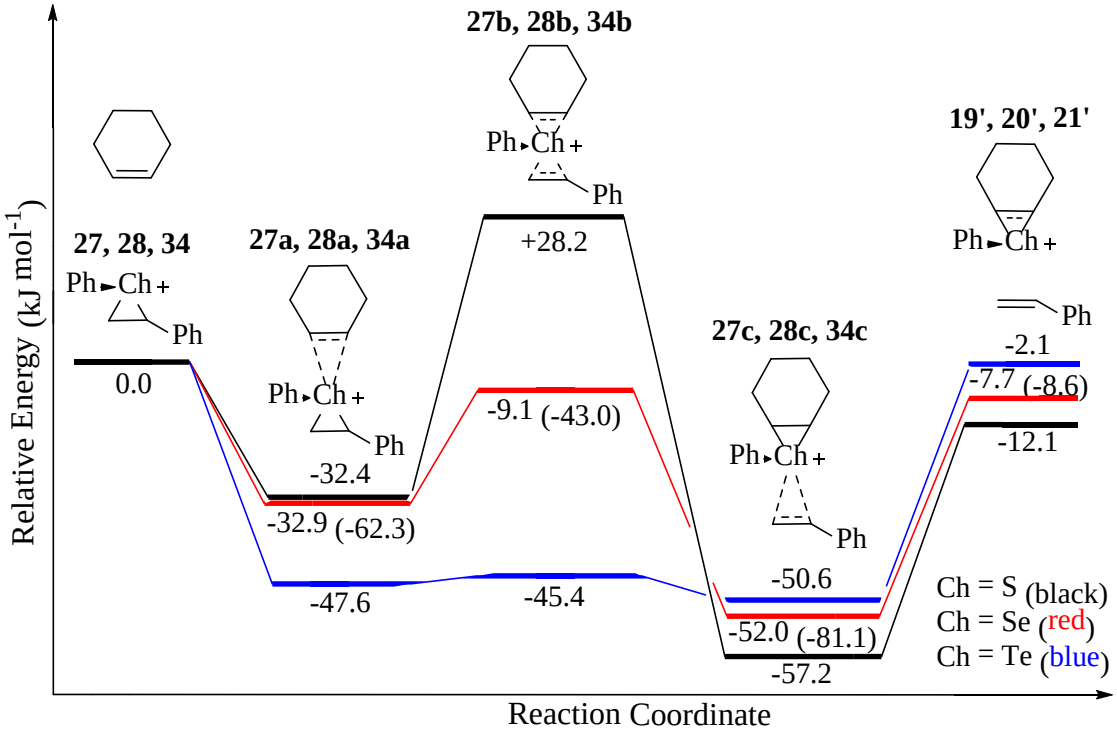

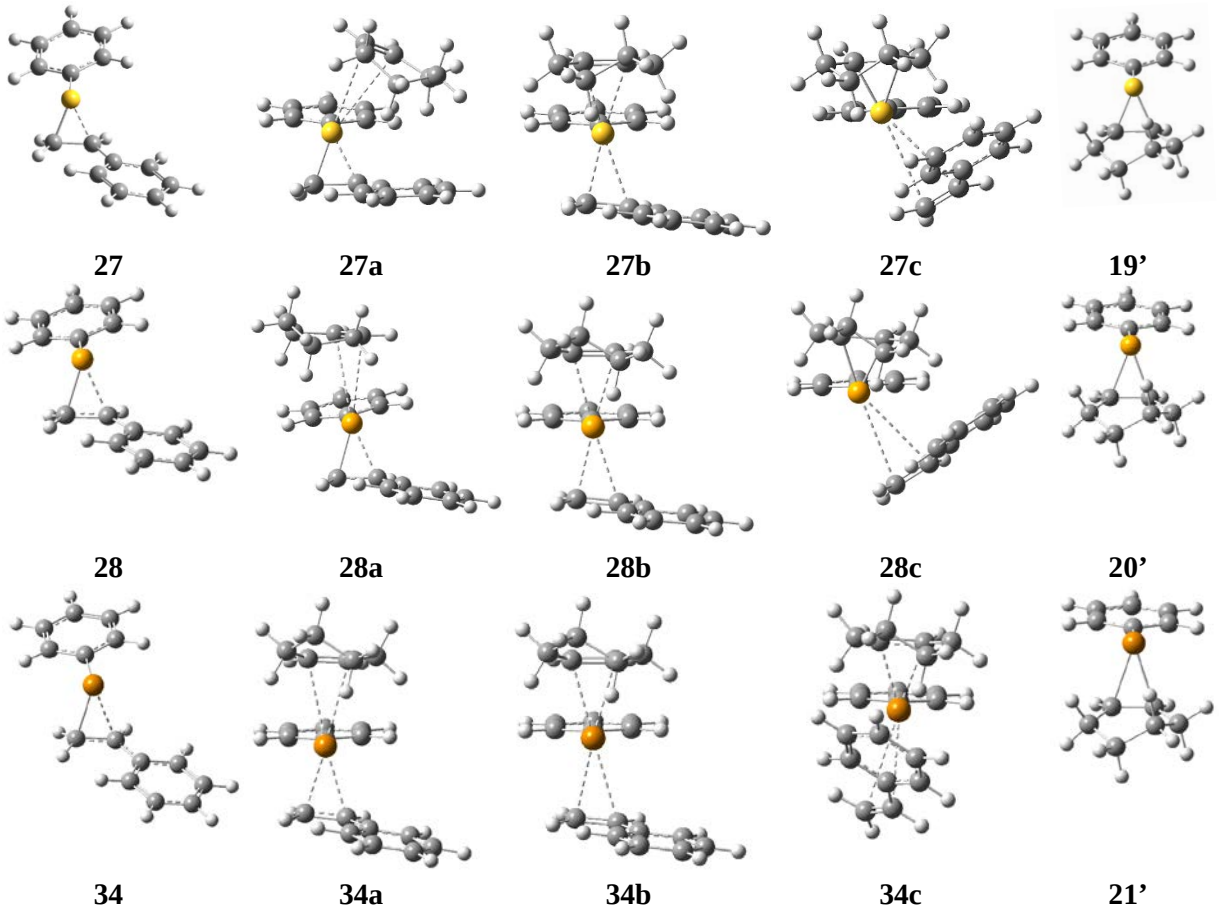

Figure 3. Relative energy diagram of **D1-3** π-ligand exchange reactions for chalcogen iranium ions **27** (adapted from reference 25), **28** and **34** with cyclohexene to afford products **19'-21'** (Ch = S – black; Se – red; Te – blue). Energies given as ΔE in kJ mol^{-1} at M06-2X/def2-TZVP relative to the free reactants. Energies in brackets correspond to previous study of Ch = Se calculated at M06/6-31+G(d), given as ΔE at 298 K in kJ mol^{-1}.[24]

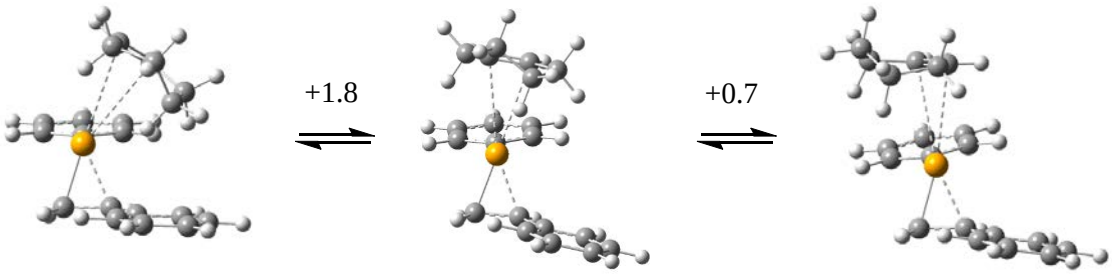

Scheme 5. Isomerisation of **28a'** to **28a** *via* transition state **28a''**. Energies given as ΔE in kJ mol^{-1} at M06-2X/def2-TZVP relative to **28a'**.

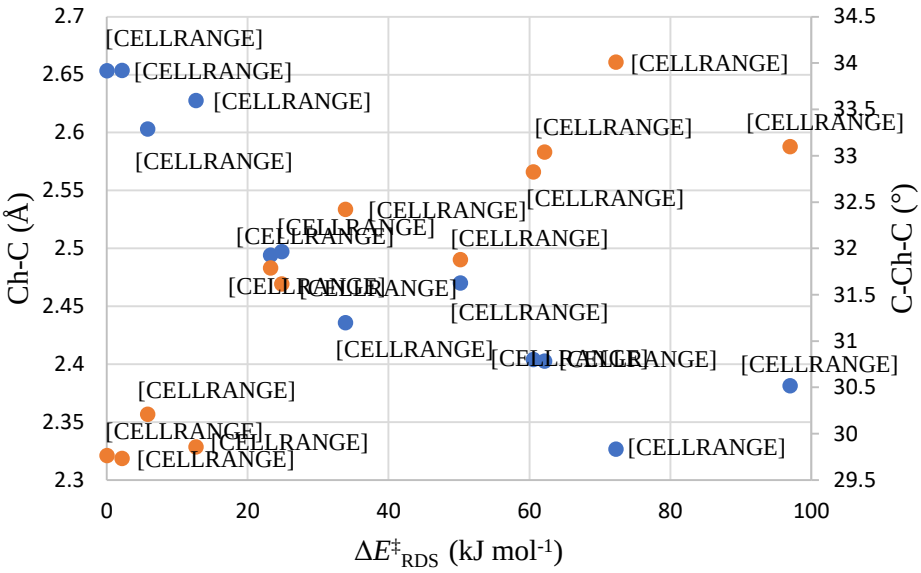

Figure 4. Plot of the average Ch-C bond length in Å (blue dots, $R^2 = 0.825$) and the average C-Ch-C angle in ° (orange dots, $R^2 = 0.808$) for transition states in reactions **A-D** against barrier height relative to association complex (kJ mol^{-1}).

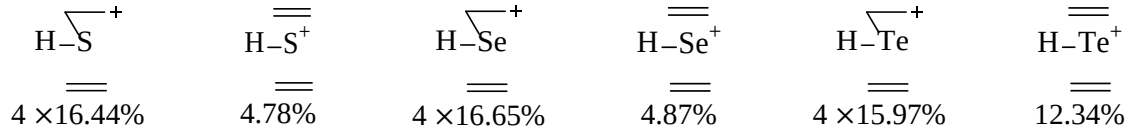

Figure 5. Selected Lewis structures from natural resonance theory analysis of transition states **31b-33b**

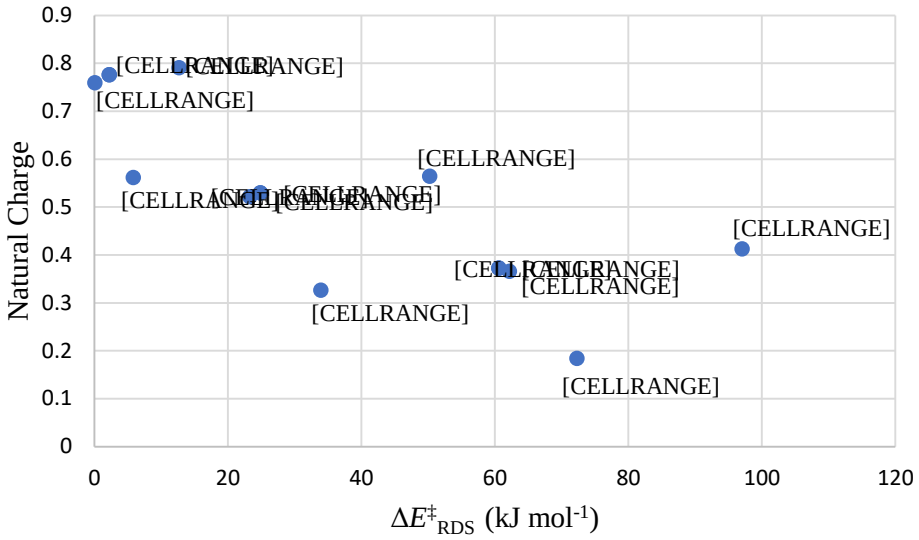

Figure 6. Plot of natural charge on the chalcogen for all transition states against barrier height relative to the association complex (kJ mol^{-1}) with $R^2 = 0.6318$.

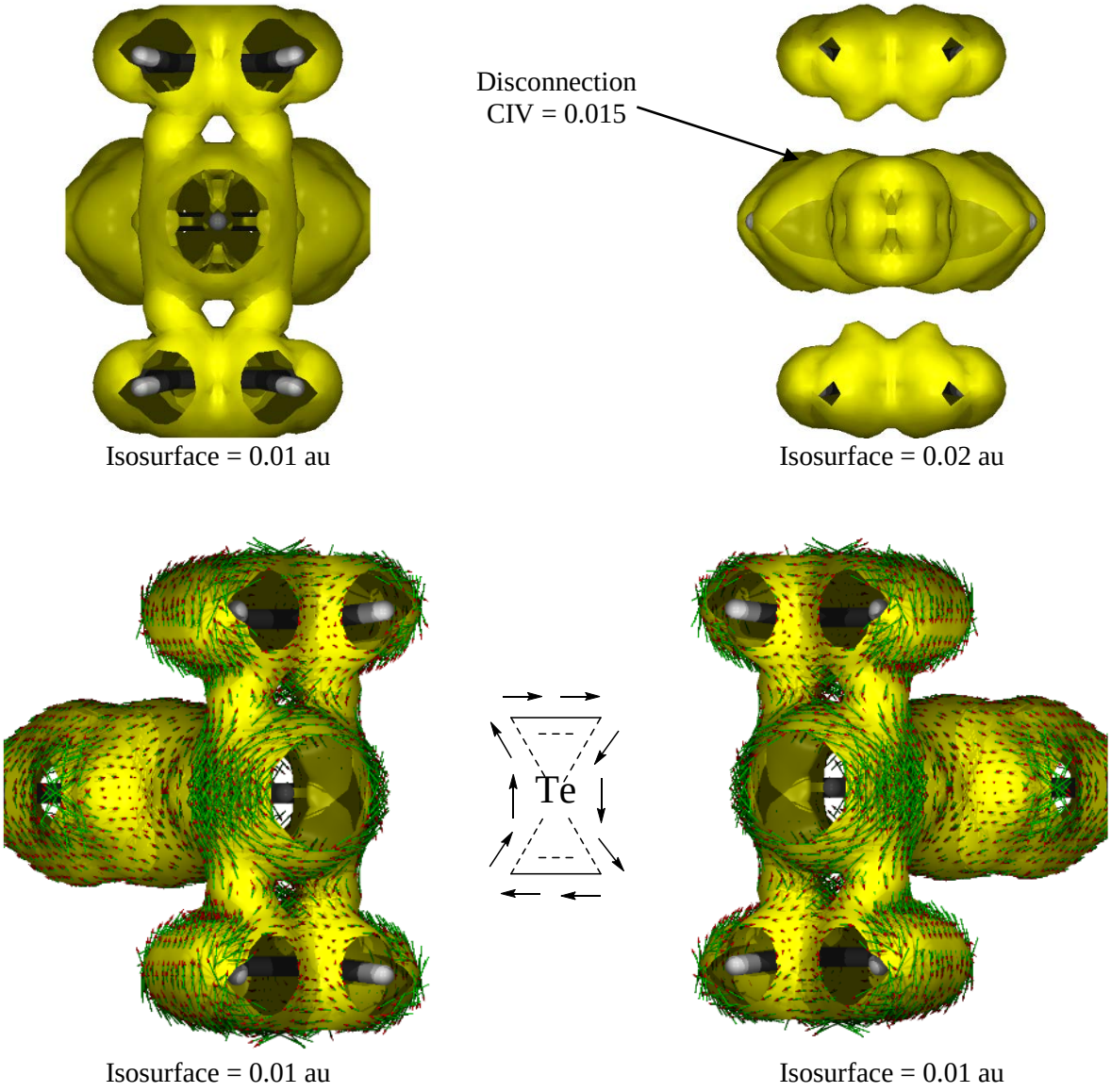

Figure 7. ACID plots at variable isosurface values of transition state **15b** from reaction **B3** involving the transfer of the $PhTe^+$ moiety between ethenes with all four of the bonds breaking/forming having a CIV value of 0.015 as indicated in the top structures. The current density vectors have been plotted on the two bottom structures to show the direction of the ring current (the right hand side has been rotated 180° around the $C{=}C_{mid}$ – Ch – $C{=}C_{mid}$ axis) with the diagram in the centre (the phenyl group points into the page and is omitted for clarity) representing the direction of electron flow as black arrows. The direction of the magnetic field lies along the Ph – Te axis pointing out of the page.

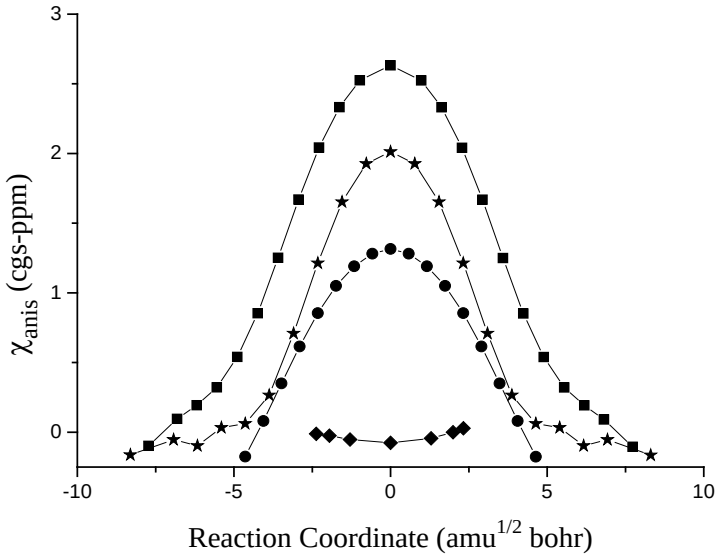

Figure 8. Change in the anisotropy of the magnetic susceptibility, χ_{anis}, (cgs-ppm) along the reaction coordinate (amu$^{1/2}$ bohr) of identity reactions **A1** (★), **A2** (■), **A3** (●) and **C3** (♦) relative to respective association complexes (raw data is collated in **Tables S4-7** in the Supporting information).

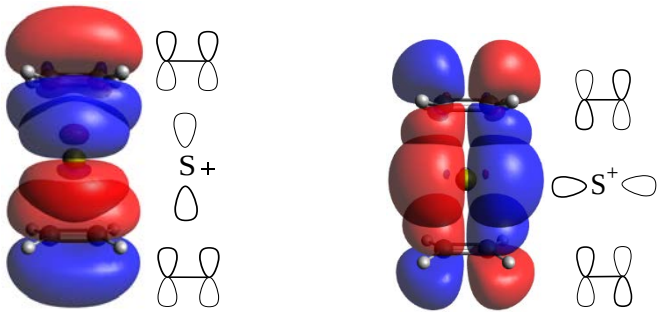

Figure 9. Significant natural bond orbital interactions in the sulphur transition state **31b** visualised at an isosurface value of 0.02 au. Hydrogens have been excluded in the schematic orbitals for clarity.